SUMMER 2021
electronics-cooling.com

electronics COOLING

FEATURED IN THIS EDITION

ALPHA | Your partner for thermal solutions

Alpha's Online Heat Sink Customization

Quickly and Easily Create a Custom Heat Sink

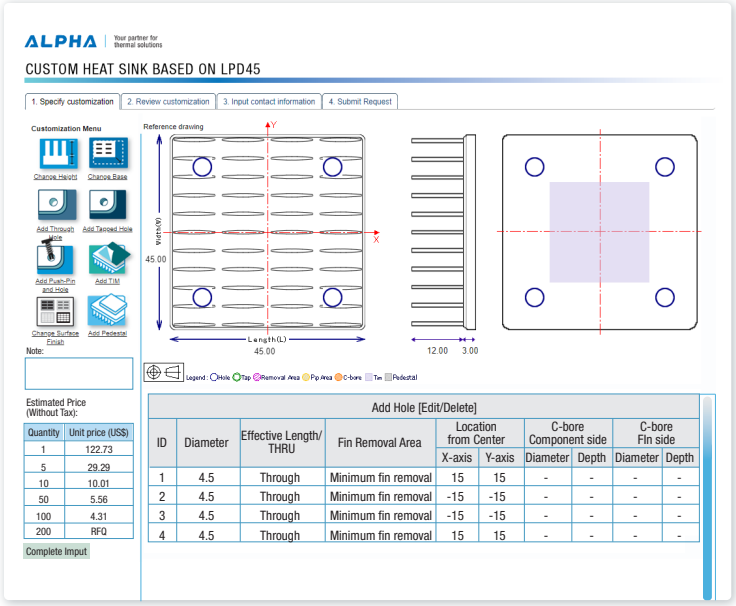

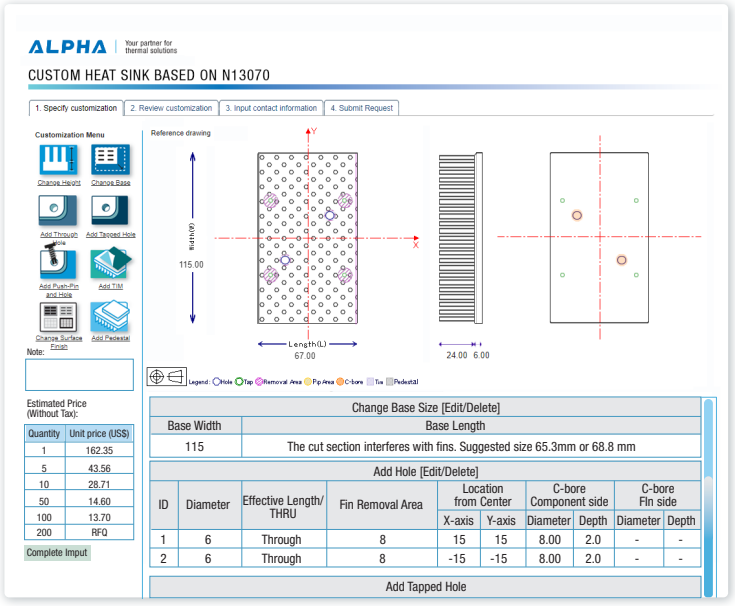

Proto Lead Time 1-2 Weeks

Typical production lead time is 2-3 weeks.

No NRE Fee

In most cases, a tooling fee will not be required.

No MOQ, No Min. Order Value

Alpha can supply from a single piece to production volumes.

Quick and Easy

A custom heat sink can be designed in minutes.

ALPHA Co., Ltd.
Head Office
www.micforg.co.jp
256-1 Ueda, Numazu City, Japan 410-0316
Tel: +81-55-966-0789 Fax: +81-55-966-9192
Email: alpha@micforg.co.jp

ALPHA NOVATECH, INC.
USA Subsidiary
www.alphanovatech.com
473 Sapena Ct. #12, Santa Clara, CA 95054 USA
Tel: +1-408-567-8082 Fax: +1-408-567-8053
Email: sales@alphanovatech.com

www.alphanovatech.com

CONTENTS

electronics COOLING
www.electronics-cooling.com

FREE SUBSCRIPTIONS

Lectrix®, Electronics Cooling®—The **2021 Spring Edition** is distributed annually at no charge to engineers and managers engaged in the application, selection, design, test, specification or procurement of electronic components, systems, materials, equipment, facilities or related fabrication services. Subscriptions are available through electronics-cooling.com.

PUBLISHED BY
Lectrix
1000 Germantown Pike, F-2
Plymouth Meeting, PA 19462 USA
Phone: +1 484-688-0300; Fax:+1 484-688-0303
info@lectrixgroup.com
www.lectrixgroup.com

CHIEF EXECUTIVE OFFICER
Graham Kilshaw | Graham@lectrixgroup.com

VP OF MARKETING
Geoffrey Forman | Geoff@lectrixgroup.com

EDITORIAL DIRECTOR
James Marengo | James@lectrixgroup.com

CREATIVE DIRECTOR
Chris Bower | Chris@lectrixgroup.com

BUSINESS DEVELOPMENT DIRECTOR
Janet Ward | Jan@lectrixgroup.com

PRODUCTION COORDINATOR
Jessica Stewart | Jessica@lectrixgroup.com

SENIOR GRAPHIC DESIGNER
Kate Teti | Kate@lectrixgroup.com

CONTENT MARKETING MANAGER
Danielle Cantor | Danielle@lectrixgroup.com

ADMINISTRATIVE MANAGER
Eileen Ambler | Eileen@lectrixgroup.com

ACCOUNTING ASSISTANT
Susan Kavetski | Susan@lectrixgroup.com

►**SUBSCRIPTIONS ARE FREE**
Subscribe online at
www.electronics-cooling.com

For subscription changes email
info@electronics-cooling.com

Reprints are available on a custom basis at reasonable prices in quantities of 500 or more. Please call +1 484-688-0300.

LECTRIX®

EDITORIAL

Victor Chiriac
Co-Editor of ECM

Dear EC Readers,

Welcome to the Summer edition of our magazine. We are happy to share with you the following articles ranging from future trends in LED driver designs, to advanced materials and liquid cooling solutions, to 5G Challenges in Data Centers. This year, we have seen a lot of progress on the Covid-19 vaccination front, with the new infection levels dropping to lower values in most of the United States. However, other countries are still fighting a significant increase in daily infections and mortality, and there is still a lot to be done at the global level. We wish everyone a healthy and productive year, and to help and assist others whenever possible and needed.

Per the latest industrial reports, there are encouraging signs that the global industry is rebounding, as new technologies are coming out on multiple fronts, spanning from medical/health, to semiconductor, to consumer electronics, data centers, automotive, etc. There are notable changes and advancements in Artificial Intelligence (AI), advanced wireless networks, quantum computing and automotive which open new frontiers for applications that were unimaginable 5 years ago. Just think where we were 5-10 years ago with the semiconductor technology nodes, then fast forward to today's most advanced ICs, which use 7 nanometer (and smaller) technology nodes, with chips of the size of a U.S. quarter or 1 Euro coin that pack over 20 billion transistors.

There are strong signals that the Covid-19 pandemic is expediting the adoption of new technologies, ranging from Machine Learning, AI, Engineering cloud technologies, while the Internet of Things (IoT) is making its way into the design space. Due to the limited mobility of the technical population, the traditional build and test activities had to be replaced by remote meetings and digital communication.

Think of the new trends in building smart, more efficient factories connected by IoT, along with advanced robots to make the assembly and testing process more efficient. And in the not so distant future, intelligent Clouds with 5G connectivity will provide the AI functionality to drive the fabrication process. Another notable trend is related to the aggressive development of smart cities that will connect vehicles with signal lights to coordinate traffic and optimize the traffic flow. As vehicles become more energy efficient, de-carbonized, safe and connected, they will be able to detect various roadblocks and construction, allowing drivers to avoid hazardous situations. AI based video analytics will help build more efficient and much safer cities.

All of these advancements require fast data transfer and large data storage, significant improvements in the related thermal management and materials solutions at the chip, package and system levels. Thermal management and cooling, materials and reliability are critical for this 4th industrial revolution driven by AI, 5G, Machine Learning. Are you working on something new and exciting? Are you converting your dreams into reality? Now is the time! We live in an unprecedented time period when the accelerating technical and medical advancements significantly impact our life and social interactions, not to mention our survival in these pandemic times.

Using our best efforts, we are all working to move forward the thermal, mechanical and materials engineering crafts through our individual and collective efforts. We hope that you will enjoy our articles and we invite you to continue to provide your feedback for our publication content improvement and suggestions for future articles and topics.

Our readers - distinguished academia and industry leaders, practicing engineers and project managers - are the voices of our thermo-mechanical community. We at *Electronics Cooling* magazine will echo and distribute your thoughts and suggestions throughout the technical and scientific electronics cooling communities. We encourage you to contribute and publish topics and articles of interest with many of our engineering peers, and to share your excellent technical achievements and further the learning of our young engineers. Wish you a fruitful and healthy remainder of 2021. Stay healthy, happy, inspired and creative!

Best regards,
Victor Chiriac

MALICO INC

If you can design it, Malico can make it.

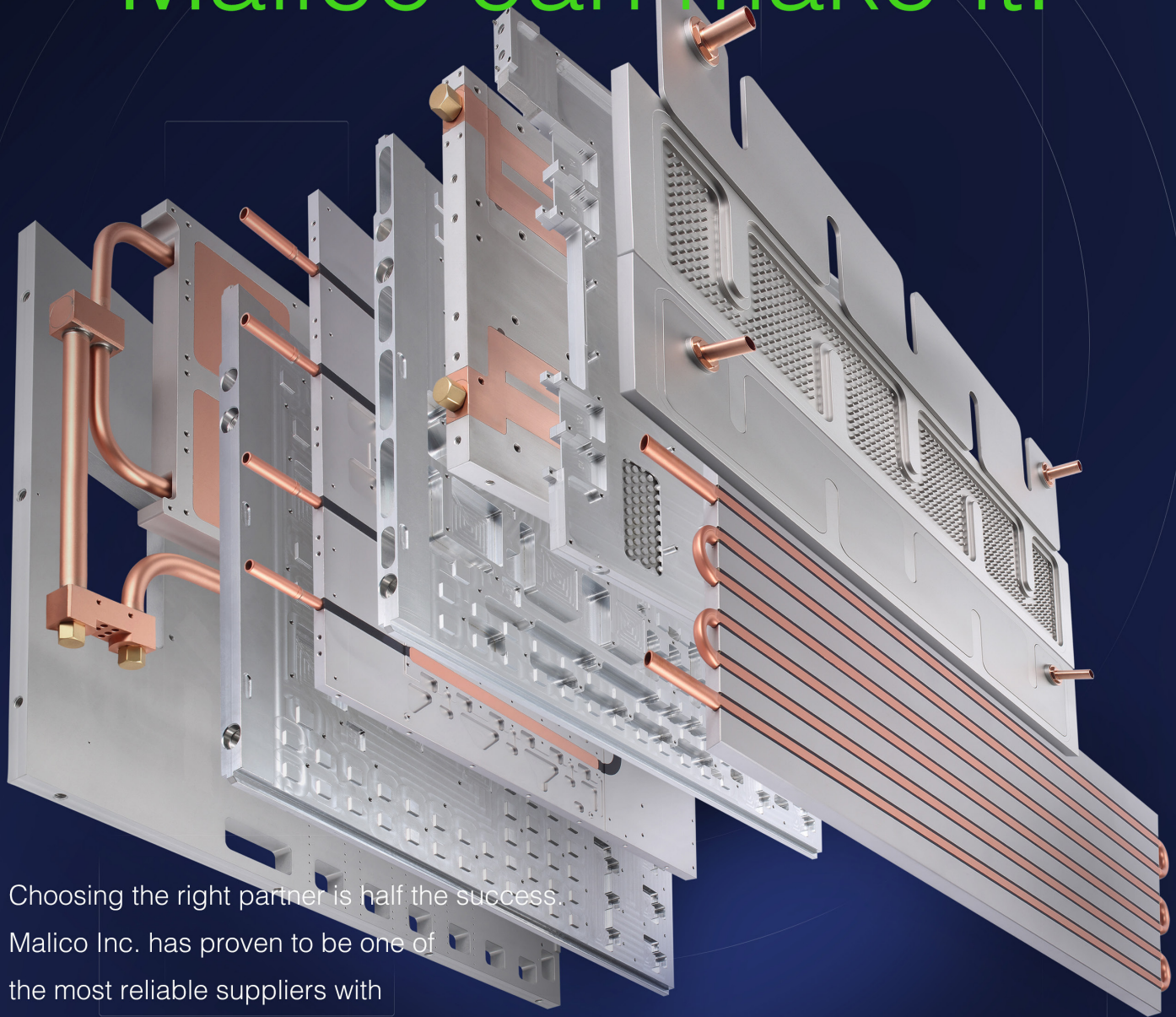

Choosing the right partner is half the success.
Malico Inc. has proven to be one of
the most reliable suppliers with
the highest quality assurance for over 38 years.

Malico Inc.

www.malico.com

5, Ming Lung Road , Yangmei District ,Taoyuan City ,Taiwan 32663
Tel :886-3-4728155
Fax:886-3-4725979
E-mail:inquiry@malico.com
Website:www.malico.com

TECHNICAL EDITORS SPOTLIGHT

Meet the 2021 *Electronics Cooling*® Editorial Board

VICTOR CHIRIAC, PhD | GLOBAL COOLING TECHNOLOGY GROUP

Associate Technical Editor

A fellow of the American Society of Mechanical Engineers (ASME) since 2014, Dr. Victor Adrian Chiriac is a co-founder and a managing partner with the Global Cooling Technology Group since 2019. He previously held technology/engineering leadership roles with Motorola (1999-2010), Qualcomm (2010 - 2018) and Huawei R&D USA (2018 - 2019). Dr. Chiriac was elected Chair of the ASME K-16 Electronics Cooling Committee and was elected the Arizona and New Mexico IMAPS Chapter President. He is a leading member of the organizing committees of ASME/InterPack, ASME/ IMECE and IEEE/CPMT ITherm Conferences. He holds 19 U.S. issued patents, 2 US Trade Secrets and 1 Defensive Publication (with Motorola), and has published over 107 papers in scientific journals and at conferences.

► vchiriac@gctg-llc.com

GENEVIEVE MARTIN | SIGNIFY

Associate Technical Editor

Genevieve Martin (F) is R&D manager for thermal & mechanics competence at Signify (former Philips Lighting), The Netherlands. She is working in the field of cooling of electronics and thermal management for over twenty years in different application fields. From 2016 to 2019, she coordinates the European project Delphi4LED (3 years project) dealing with multi-domain compact model of LEDs. She served as General chair of Semitherm conference and is an active reviewer and technical committee in key conferences Semi-Therm®, Therminic, Eurosime.

► genevieve.martin@signify.com

ROSS WILCOXON | COLLINS AEROSPACE ADVANCED TECHNOLOGY

Associate Technical Editor

Dr. Ross Wilcoxon is a Technical Fellow in the Collins Aerospace Advanced Technology group. He conducts research and supports product development related to component reliability, electronics packaging and thermal management for communication, processing, displays and radars. He has more than 40 journal and conference publications and is an inventor on 30 US Patents. Prior to joining Rockwell Collins (Now Collins Aerospace) in 1998, he was an assistant professor at South Dakota State University.

► ross.wilcoxon@collins.com

COOLING EVENTS

News of Upcoming 2021 Thermal Management Events

OCT
19-20

THERMAL LIVE™
Online Event

Electronics Cooling's Thermal LIVE™, the world's largest online thermal management event, returns for its 7th year this October. The two-day program features experts in the thermal management field, presenting live educational sessions on industry challenges, trends, and products. Past topics have included advanced thermal techniques in power electronics, design and manufacturing of blind mate couplings, selecting TIMs for different applications, calculations and design elements for liquid cooling, and more.

If you're an electronics or mechanical engineer who works with thermal management, this event is a can't-miss.

Desc. source: electronics-cooling.com
► https://thermal.live/

NOV
15-19

SC21
America's Center | St. Louis, Missouri

The international conference for high performance computing, networking, storage, and analysis. Expand your knowledge, enrich your experiences, and network with others in the HPC community. Take in technical presentations, papers, workshops, tutorials, posters, and Birds of a Feather sessions. Explore exhibits showcasing the latest innovations from the world's leading manufacturers, research organizations, and universities. And, enjoy exploring our host city St. Louis. Journey to the top of the Gateway Arch!

Desc. source: electronics-cooling.com
► https://sc21.supercomputing.org/

NOV
16

THERMAL MANAGEMENT INNOVATION USA
TCF Center | Detroit, Michigan

The Annual BEV Thermal Management Innovation USA Congress, Detroit is the number one event to match buyer requirements with expert solutions during the Automotive sector's battery evolution. Following on from the tremendous success of the previous three events, Thermal Management Innovation USA has firmly established itself as the automotive industries first-class event to gain a clear and pragmatic view of the key challenges and current need to know learning objectives surrounding advanced battery thermal management systems; to increase efficiency, range, battery health, and optimize solutions for increasingly demanding advanced charging requirements.

Desc. source: electronics-cooling.com
► www.battery-thermal-management-usa.com

Advective Thermal Resistance

Ross Wilcoxon
Associate Technical Editor for *Electronics Cooling*
Collins Aerospace

A previous *Electronics Cooling* Magazine article, which discussed the process for analyzing the thermal performance of cooling fans [1], mentioned the need of accounting for the increasing coolant temperature as air passes through a heat sink. That article used an 'average' air temperature, which was defined as the midpoint between the inlet and outlet air temperatures. This article discusses that approach, as well as an alternate method that is more physically robust.

When a system is cooled with a fluid, the fluid temperature rises as it passes through the system and absorbs energy through convective heat transfer. The larger the power dissipation or smaller the mass flow rate, the greater the rise in coolant temperature. As the coolant temperature increases, a higher surface temperature is needed to dissipate the same power with the same convection coefficient. This increases the overall thermal resistance compared to a system in which the fluid temperature remains constant.

One method of accounting for this 'advective' thermal resistance is to assume that the average coolant temperature is the midpoint between the inlet and outlet coolant temperatures. As long as the cooling fluid remains single phase (i.e., no boiling), the outlet coolant temperature, To, depends on the inlet fluid temperature (T_i), the fluid's specific heat (c_p), the coolant flow rate ($\dot{m}$), and the power dissipation (Q) as shown in *Equation 1*.

$$T_o = T_i + \frac{Q}{\dot{m}c_p}$$

Equation 1

If we assume that the representative coolant temperature is the midpoint between the inlet and outlet temperature (T_{mid}) = (T_o + T_i)/2, we can analyze the convective heat transfer to determine the temperature of the heat transfer surface ($T_{surface}$), which is assumed to be uniform, using *Equation 2*.

$$Q = hA\left(T_{surface} - T_{coolant}\right) = hA\left(T_{surface} - T_{mid}\right) = hA\left(T_{surface} - \left(T_i + \frac{Q}{2\dot{m}c_p}\right)\right)$$

Equation 2

While this approach to account for the coolant temperature rise is often quite accurate, it is an approximation because it assumes that the average coolant temperature is the same as the midpoint value. One can recognize the limitation of this assumption by considering a situation in which a coolant enters a tube that has a constant surface temperature. If the tube is only a meter long, it may be reasonable to assume that the appropriate typical temperature of the coolant as it flows past the tube surface is close to the midpoint temperature. However, if that same uniform-temperature tube is 10km long, it is likely that the fluid would essentially be at the tube temperature well before the end of the tube and, therefore, the average fluid temperature would be closer to the tube surface temperature. The accuracy of the midpoint temperature assumption shown in *Equation 2* depends on a combination of the mass flow of fluid and the convective thermal resistance (heat transfer coefficient and amount of heat transfer area).

A more general approach to account for the advective thermal resistance is to turn to methods developed for fluid-to-fluid heat exchangers. The effectiveness-NTU method relates the effectiveness of a heat exchanger, ε, to the number of thermal units (NTU). The effectiveness, which is defined as the actual heat transfer between fluids divided by the maximum possible heat transfer between fluids, i.e., $\varepsilon = q_{actual}/q_{maximum\ possible}$, is a function of the heat exchanger configuration and the flow rates and specific heats of the two fluids. The NTU for a system is defined as $NTU = UA/(\dot{m}c_p)_{minimum}$, where $\dot{m}c_p$ is the fluid mass flow rate times its specific heat; the 'minimum' subscript indicates that the fluid with the smaller value of $\dot{m}c_p$ is used to calculate NTU. The term UA is the inverse of the overall thermal resistance between the two fluids, including convection coefficients for both fluids, fin efficiencies, and conduction through the solid materials that separate the two fluids.

A number of relatively complex equations have been developed to calculate the effectiveness of heat exchanges with different geometries, configurations, etc. Fortunately for those of us who work in the area of electronics cooling, we generally do not need to deal with them. When there is only a single fluid involved, the effectiveness is simply $\varepsilon = 1 - e^{-NTU}$. This equation allows us to easily account for the effect of advective thermal resistance to determine the heat transfer from a surface, which is assumed to be at a uniform temperature, to a fluid with a known inlet temperature. The UA term in the NTU calculation is the inverse of the thermal resistance, $R_{thermal} = 1/hA$, where h is the convection coefficient and A is the effective surface area that accounts for fin efficiency.

Consider, for example, a 10 cm diameter tube that is held a fixed temperature of 100°C. Air at atmospheric pressure enters the tube at 25°C and an average velocity of 1 m/s. Ignoring the effects of developing flow, the convection coefficient is constant so the heat transfer to the air is only dependent on the tube length, which dictates the area available for heat transfer. *Figure 1* shows the heat transfer calculated for this situation using three different assumptions on the coolant temperature (the equations that were used for these calculations are summarized in *Table 1* later in this article). For 'Constant Coolant Temperature', it is assumed that the cooling air temperature is the inlet air temperature throughout the tube. For 'Coolant Midpoint Temperature' the average coolant temperature is assumed to be the midpoint of the inlet and outlet coolant temperatures (using *Equation 2*). The 'Effectiveness-NTU' results correspond to using the heat exchanger ε-NTU approach for calculating the heat transfer. This figure also shows the values of NTU calculated for the conditions considered in this analysis.

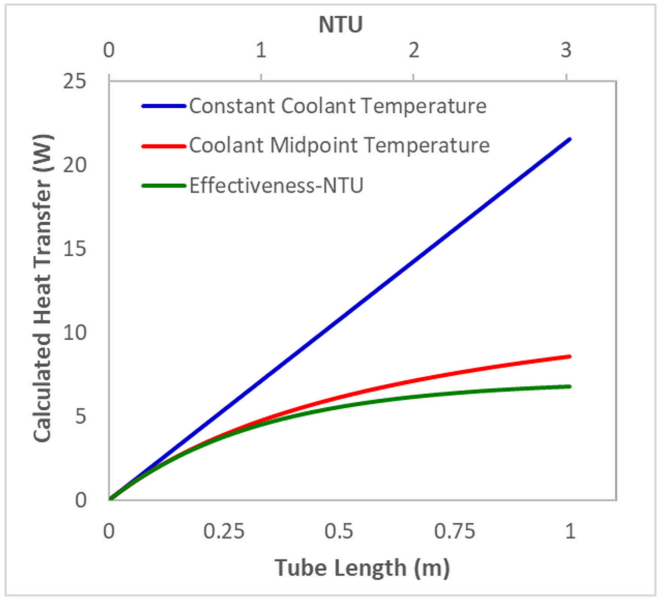

Figure 1. Calculated heat transfer to air flowing through a tube

Figure 1 shows that at low enough values of NTU, which may be due to high thermal resistance (in this case, a short tube with relatively small heat transfer area) or large mass flow rates, all three approaches predict similar values for heat transfer. But as the length of the tube increases (the NTU becomes larger), there is substantial error associated with assuming the coolant temperature remains constant. Eventually, at a large enough NTU the midpoint temperature assumption also demonstrates increasing error. Physically it is logical that the heat transfer would eventually asymptote to a fixed value as the tube becomes long enough and the coolant temperature approaches the wall temperature; this behavior is only demonstrated by the calculations using the Effectiveness-NTU method.

One can estimate when and whether the effectiveness-NTU method is needed for an accurate calculation by comparing the heat transfer calculated with the other methods to that calculated using ε-NTU. Defining the calculation error as $E = (Q\text{-}Q_{\varepsilon\text{-NTU}})/Q_{\varepsilon\text{-NTU}}$, the error associated with assuming constant coolant temperature is:

$$E_{constant\ coolant\ temp} = \frac{\frac{(T_s-T_i)}{R_{th}}}{\dot{m}c_p(T_s-T_i)*(1-\exp\left(-\frac{1}{R_{th}\dot{m}c_p}\right)} - 1 = \frac{NTU}{1-\exp\left(-NTU\right)} - 1,$$

Equation 3

where R_{th} is the heat sink thermal resistance and $NTU = (hA)/(\dot{m}c_p) = 1/(R_{th}\,\dot{m}c_p)$.

Likewise, the error associated with using the midpoint coolant temperature can be calculated using:

$$E_{midpoint\ temp} = \frac{\frac{(T_s-T_i)}{\left(R_{th}+\frac{1}{2\dot{m}c_p}\right)}}{\dot{m}c_p(T_s-T_i)*\left(1-\exp\left(-\frac{1}{R_{th}\dot{m}c_p}\right)\right.} - 1 = \frac{NTU}{(NTU+0.5)*(1-\exp(-NTU))} - 1$$

Equation 4

These two error values are plotted in *Figure 2*. This shows, that at a high enough flow rate or thermal resistance, one can assume that the flow rate temperature is either fixed or equal to the midpoint temperature. However, at low flow rates, those assumptions can lead to significant errors.

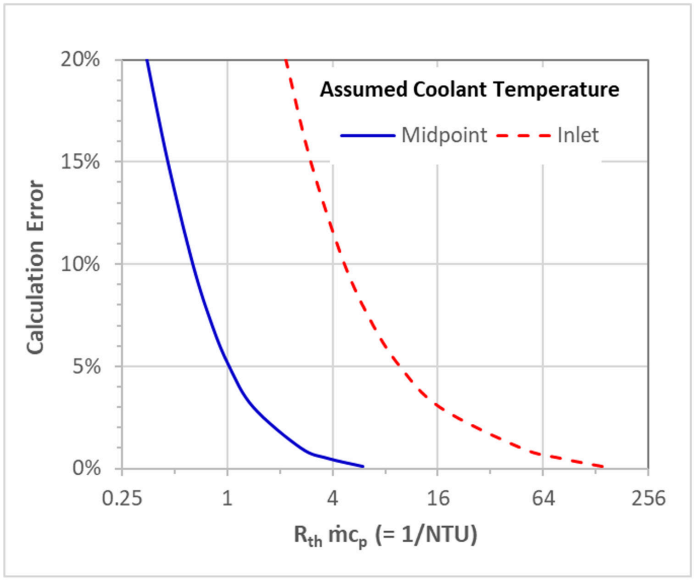

Figure 2. Comparing errors of different assumptions for coolant temperature

Table 1 summarizes the equations that can be used to determine the heat transfer (for a known heat sink surface temperature) or the heat sink temperature (for a known heat dissipation) with different approaches to account for the advective thermal resistance. This table also shows what inverse NTU (thermal resistance multiplied by the coolant mass flow rate times its specific heat) at which the calculation would be within ~5% of the correct value calculated using the NTU-Effectiveness method.

Analysis Approach	Heat Dissipation, Q (surface temperature is known)	Surface Temperature, Ts (heat dissipation is known)	95% accuracy: $R_{th}\dot{m}c_p \geq$
Constant Coolant Temperature	$Q = \frac{(T_s - T_i)}{R_{th}}$	$T_s = T_i + R_{th}Q$	~10
Midpoint Coolant Temperature	$Q = \frac{(T_s - T_i)}{(R_{th} + \frac{1}{2\dot{m}c_p})}$	$T_s = T_i + (R_{th} + \frac{1}{2\dot{m}c_p})Q$	~1
Effectiveness-NTU Method	$Q = \dot{m}c_p(T_s - T_i) * (1 - \exp\left(-\frac{1}{R_{th}\dot{m}c_p}\right)$	$T_s = T_i + \frac{Q/\dot{m}c_p}{(1 - \exp(-\frac{1}{R_{th}\dot{m}c_p})}$	0
T_s = heat sink surface temperature, T_i = coolant inlet temperature, R_{th} = 1/hA, $\dot{m}$ is the coolant mass flow rate, c_p is the coolant specific heat (~1000 J/kgK for air)			

Table 1. Heat transfer & surface temperature equations for different advective thermal resistance approaches

SUMMARY

This article described approaches that can be used to account for the additional thermal resistance due to the coolant temperature increasing as it passes through the system it is cooling. The magnitude of this effect depends on the coolant properties (specific heat), its flow rate, and the thermal resistance of the system it is cooling. At low flow rates or high thermal resistance, it is acceptable to assume that the coolant temperature remains constant or to use the midpoint coolant temperature. However, the NTU-Effectiveness approach that was described here should be applicable to any situation.

REFERENCES

1. Ross Wilcoxon and Genevieve Martin, "Fan Cooling – Part 1: Determining Flow Rate", *Electronics Cooling* Magazine, Spring 2021, pp. 6-9

Vladimir Székely (1941-2020)

Dr. Vladimir Székely, a former head of the Department of Electron Devices of the Faculty of Electrical Engineering and Informatics of the Budapest University of Technology and Economics (BME), professor emeritus, full member of the Hungarian Academy of Sciences, died silently after a long-suffering illness in November 2020.

He was the developer of the Network Identification by Deconvolution (NID) method, which has enabled the Structure Function methodology, opening new avenues in thermal transient testing methodologies of semiconductor device packages.

Vladimír Székely was one of the outstanding electrical engineers of our time and one of the most significant lecturers of the Faculty of Electrical Engineering and Informatics of BME besides being one of the most referred researchers of BME. This can be proved by the thousands of Hungarian electrical engineers he taught about the physics and application of electronic devices and the basics of microelectronics. Students who have been taught the use of computer methods in engineering design for decades by him, or those who have been introduced to the basics of image processing will remember his lectures in all their life. His research activity was acknowledged by the Harvey Rosten Award in 2000, and his outstanding work was recognized with prestigious prizes and honours in Hungary (Academic Prize: 2002, Albert Szent-Györgyi Award: 2006, Denis Gábor Award: 2010).

Vladimir was a blood innovator, in the most positive sense of the word, in both education and research. He introduced new, programmed teaching methods into university education, decades ahead of his age and ahead of computers. His former students still remember the precision and thoughtfulness of their lectures as a model of university education. He was one of the approx. 5 BME instructors, who were the first to get acquainted with computer programming and were the first to start teaching computer programming at BME. Together with his fellow professor, Kálmán Tarnay, they developed the TRANS-TRAN circuit simulation program in Hungary - at the same time as the first version of the SPICE program - with which thousands of electrical engineering students learned the basics of computer circuit design. And this tool has treated already also the thermal effects, which was his special interest.

In addition to his teaching work, especially in the last 25 years, he has gained a very significant international reputation for his achievements in researching the thermal behaviour of semiconductor devices and microelectronic systems. He led the work of his research group in about 15 research projects carried out in international cooperation, advancing the reputation of the knowledge of Hungarian engineers.

Practical work has always been central to his interest. In order to utilize the research results of the research group led by him, together with colleagues he established the spin-off company of the Department of Electronic Devices of BME, MicReD Ltd., which is now part of SIEMENS Digital Industries. He was the CTO of MicReD for about 15 years. Over the past decades, the products developed by him or under his control have become world-famous in the field of thermal qualification of integrated circuits and systems. In the last few years, the thermal transient tester and the measurement procedure based on the evaluation of structure functions has become a de facto standard for solid-state lighting technology, used by most of the leading companies in the solid-state lighting industry. To crown scientific and market success, the EIA JEDEC JC15 Standardization Committee, on a proposal from leading semiconductor manufacturers, adopted a test and modelling method based on thermal transient measurements and the use of structure functions as a standard.

All the activities of Vladimir Székely were characterized by a wealth of ideas. He patented a new principal printing device aimed for micro-computers about 35 years ago, and developed a prototype of a cash register that used it.

He often combined methods from different engineering domains in a surprising manner. He developed the algorithms of two thermal simulation programs which were also commercially available, using novel and original solutions: image processing combined with circuit theory, image processing and signal processing algorithms combined with thermal engineering. These approaches were used not only in his novel thermal simulation methods but were part of, for example, a liquid crystal-based thermography system. These unusual combinations of basic principles also resulted in solutions far from thermal problems, e.g., his fingerprint recognition algorithm is still frequently cited today.

His new simulation methods and algorithms have always been verified by actual physical measurements. An early example (dating back to circa 1972 - 1976) is the study of the influence of thermal feedback on the electrical characteristics of OpAmps, which included both electro-thermal circuit simulation and different physical experiments and measurements, such as liquid crystal-based thermography, frequency domain measurement of the output impedance, etc.

The peculiarity of Vladimir Székely's work is that the role of hardware and software elements is the same in them. Every piece of equipment he designed is based on some witty, new process, a novel engineering approach to a problem that no one has ever used before.

Unfortunately, his well-known long term illness has prevented him from directly participating in teaching and research for some years now, but his sentences are still mentioned today by his former students and colleagues, who will remember him forever.

Rest in peace Vladimir.
Marta Rencz, Andras Poppe

Structure Functions: The Universal Tools for Thermal Design, Testing and Quality Control

Gábor Farkas
SIEMENS Digital Industry Software STS MA, Hungary

Márta Rencz
Budapest University of Technology and Economics

Near the end of the 20th century, increasing power levels became the primary challenge in system design, which triggered a complex response from electrical, mechanical and material engineers. The combination of thermal measurements and thermal simulation helped achieve thermally aware system designs. However, no real solution was known for the valid comparison of thermal design concepts and for identifying failure locations in actual samples during quality control. Simulation attempts often failed because the thermal material parameters from data sheets significantly differed from the actual behaviour of thin material layers which typically build up power packages and modules.

Breakthroughs often occur all of a sudden. In the 1980's, Professor Vladimír Székely studied a set of measurements of the temperature change in time of an assembly after applying a sharp power step on it. Three samples of the same manufacturing lot were tested.

It was obvious in this plot (*Figure 1*) that, for the first ~ half second the heat still propagated in the internal sandwich-like structure of the sample, through the silicon chip, on which power was applied, then through various layers of the investigated packaged device. After this half a second, the heat penetrated into the thermal paste (thermal interface layer, TIM) between the sample and the test bench. The screws that provided the fixing force to the sample were not tightened equally, leading to different thicknesses of the thermal paste in the three cases. Structural changes caused a difference in the thermal transient behaviour.

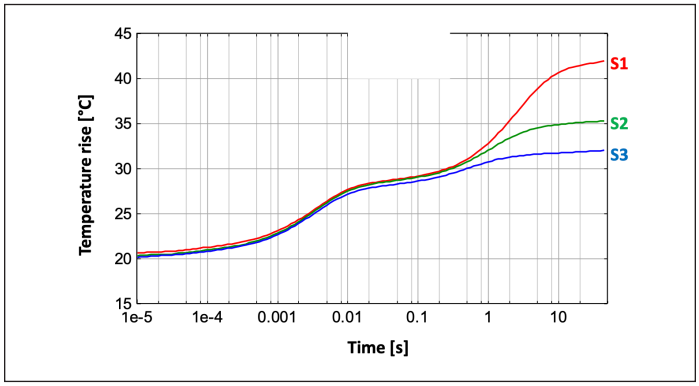

Figure 1. Temperature change on three samples of the same manufacturing lot after applying a sharp power step

It has long been known that, in thermal measurements, a very stable measurement arrangement must be ensured in order to achieve repeatability. Changes in the structure of the arrangement induce changes in the temperature response. In a conventional interpretation of the data, the measurement of sample S3 in *Figure 1* is good while the two other measurements are wrong. However, in considering the results differently, the dissimilarity in the measurement results is not considered to be the problem but is instead the solution needed for addressing the problems of measurement repeatability, as outlined above.

Gabor Farkas
Dr Gábor Farkas is Technical Manager at Siemens D in Budapest.
He received his MSc and PhD in electronics engineering from the Budapest University of Technology and Economics (BME), Hungary. Since 2000 he has worked for MicReD. His main field has been developing hardware and software tools and measurement technologies for thermal characterization of semiconductor devices. He participates in research on wide band gap devices and power LED devices. He is also an associate professor at BME. He has published over 60 technical papers in journals and in conference/workshop proceedings. He is the author of chapters in technical books on integrated circuit design, measurement of power modules, LED and wide band gap devices.

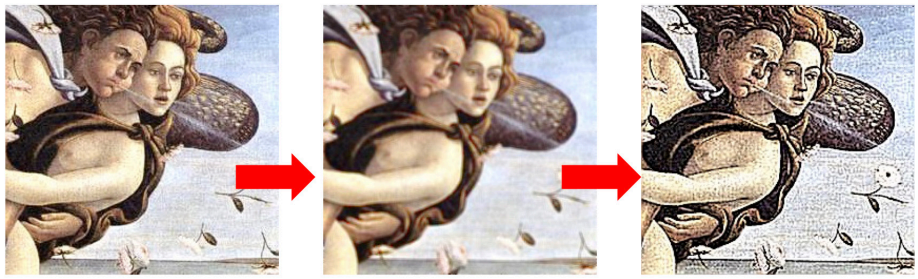

(a) (b) (c)

Figure 2. Convolution in space (blurring) and deconvolution to restore the original picture

V. Székely was an expert on the theory of filters and a renowned authority on image processing techniques. He knew how smudged pictures can be restored to original sharpness. A defocused camera causes a blurring of pictures, that is, the content of a pixel is superposed on the neighbouring pixels by a certain weight. This is operation is known as convolution in space, a two-dimensional filter smashes the picture content over the image (*Figure 2 a* to *b*).

The process is a linear transformation; it can be reversed by a deconvolution procedure (*Figure 2 b* to *c*). The theory of linear systems provides several algorithms for this operation, such as Fourier transform or iterative methods.

Prof. Székely realized that the bumpy response curve of the device under test and the measurement environment is the convolved signal of the sharp power step, at the output of a low pass filter [1].

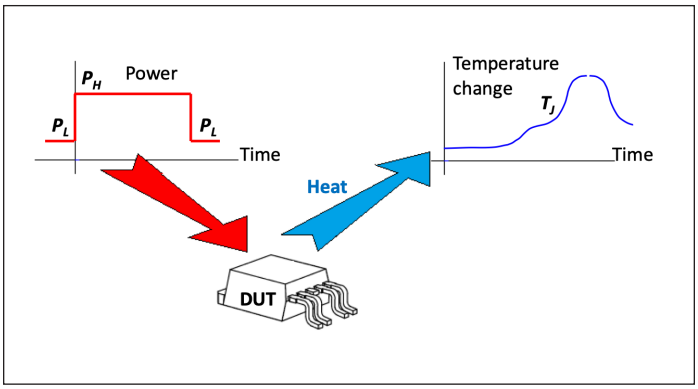

Figure 3. The scheme of thermal transient testing, sharp power changes in time produce a characteristic bumpy temperature change curve.picture

The different layers in the structure have various geometries and thermal parameters, such as thermal conductivity and specific heat. These can be represented by a dense net of thermal resistances and thermal capacitances, with one or more entry points of the heat (driving points) (*Figure 4*). Thermal capacitances cause a delay in the temperature increase because they can temporarily store the thermal energy.

In *Figure 2*, a known filter (the aperture of the defocused optics) blurred the picture. The same known filter can be used to restore the original from the convolved, blurred one in a reverse process.

For the convolution in time, which produces the bumpy curve at the output of a thermal resistance-capacitance (RC) network, the players in the scheme are again: an input signal, a filter and a convolved output signal. However, the target is now different: in the deconvolution scheme, the filter is the unknown that must be determined:

- from the known input signal: the waveform of the applied power step and
- from the output signal: the measured temperature change.

Some measurement apparatus is needed to apply the power and to record the temperature change, but no external source (x-ray or acoustic) is needed for the investigation. The structure of an assembly can be identified using the inherent temperature changes in the system.

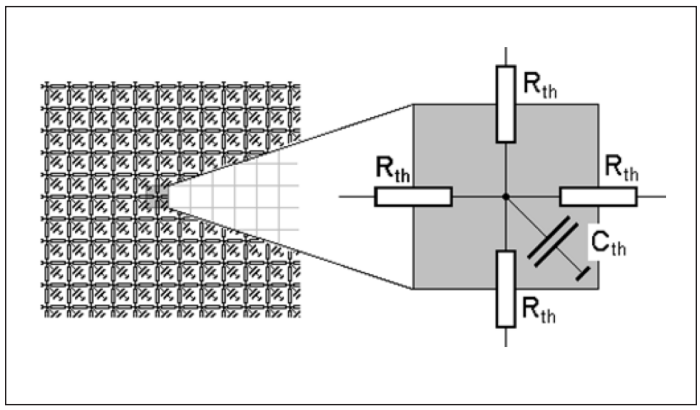

Figure 4. Equivalent thermal RC net of an object characterized by its geometry and its thermal resistances and thermal capacitances

Although the convolution theory and the use of RC filters seem to be distant from the practical discipline of thermal transient testing, it is easy to find a common denominator between them: the theory of linear systems. In the typical temperature range of use, most non-linear effects (radiation, nonlinearity of thermal conductivity) can be neglected.

Thermal conduction is dominated by a blend of two mechanisms, heat propagation through an elementary slice (*Figure 5*) and internal energy growth due to heat flow into the slice (*Figure 6*).

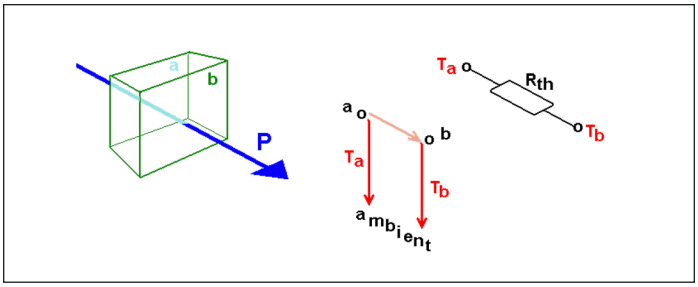

Figure 5. Heat flow through a material slice

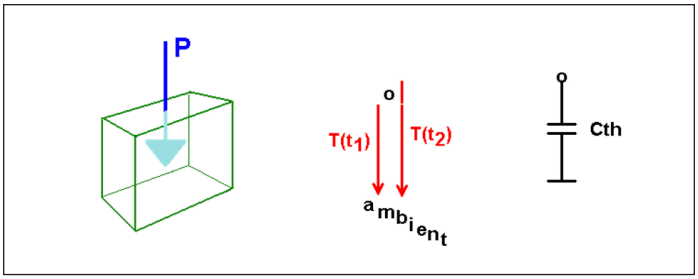

Figure 6. Heat flow into a material slice

The theory of linear systems claims that the system corresponding to *Figure 4* behaves in the same way as a reduced set of thermal resistances and capacitances arranged in one of the configurations shown in *Figure 7*.

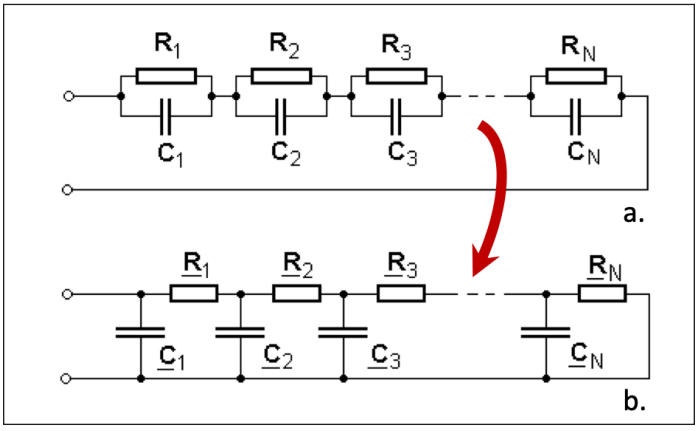

Figure 7. Foster (a.) and Cauer (b.) type filter representation of discretized structures

Actual thermal systems correspond to the complex RC net of *Figure 4*. In a test, P(t) power is applied at some thermally connected nodes and terminated by constant temperature at their boundaries. In case constant Pon power is switched on at zero-time (step function), a single series RC element in *Figure 7a* will produce exponential temperature increase after switching on the power (current), adding $T(t) = P_{on} \bullet R \bullet (1 - e^{-t/\tau})$ temperature (voltage) term to the chain response. The R *magnitude* denotes the thermal resistance of the fragment; $\tau = R \bullet C$ is a time constant where C is the thermal capacitance. Accordingly, at the input (in this case at the junction) we get a *sum* of exponential functions,

$$T(t) = P_{on} \cdot \sum_{i=1}^{n} R_i \cdot \left(1 - e^{-t/\tau_i}\right) \qquad (1)$$

Different material slices have different characteristic thermal parameters, the resulting different R magnitudes and τ time constants make the T(t) curve "bumpy", as seen in *Figure 1*.

In a fine net of series RC chain stages, *Equation (1)* approximates an integral

$$T(t) = P_{on} \cdot \int_0^{\infty} R(\tau) \cdot \left(1 - e^{-t/\tau}\right) d\tau \qquad (2)$$

The formula says that the system response is the convolution-like integral of an R(τ) time constant spectrum and a fixed f(t)=1 – $e^{-t/\tau}$ function. The inverse of (2) can be produced in an iterative numerical process. The mathematical apparatus of such a deconvolution procedure yielding R(τ) is rather complex; a rigorous treatment of it is described in [2]. The procedure is called Network Identification by Deconvolution, NID method.

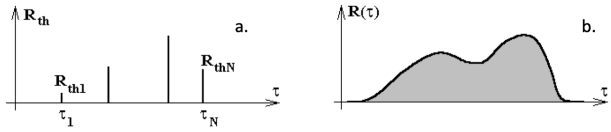

Figure 8. Time constants in a lumped element system (a) and in a distributed parameter system (b)

Before the advent of the NID method, the measured curved could be approximated by 3-4 time constants that can be determined with curve fitting. The NID method easily yields several hundred RC stages and produces a fine resolution equivalent scheme of the structure.

Discrete time constants (*Figure 8a*) or their spectrum (*Figure 8b*) can be produced with this process from a measured T(t) curve, but the equivalent RC network corresponds to *Figure 7a*, which is a behavioural model only.

In the physical reality, *Figure 5* illustrates the temperature drop across a material slice. In *Figure 6*, T_1 and T_2 temperatures are measured from the ambient, a C_{th} thermal capacitance appears between a point representing the material portion and the ambient.

Serial *RC* chains (*Figure 7a*) can be converted to *RC* ladders (*Figure 7b*) by the Foster – Cauer transformation known in linear circuit theory (see e.g., Annex C in [3]). These two processes (the exponential decomposition by deconvolution and the Foster – Cauer transformation in a sequence), provide a direct synthesis method for transforming measured transients into a one-dimensional physical compact model of the complex thermal system.

The structure function (*Figure 9*) is an excellent graphic tool to characterise the heat conducting path. In the ladder of *Figure 9b* this chart sums up the thermal resistances, starting from the heat source (junction) along the x-axis and the thermal capacitances along the y-axis.

A *low gradient* section in the structure function means that, at

the corresponding structural detail, even a small volume such as a thin material layer that has low thermal capacitance causes large change in thermal resistance. These regions have *low thermal conductivity* or *small cross-sectional area*.

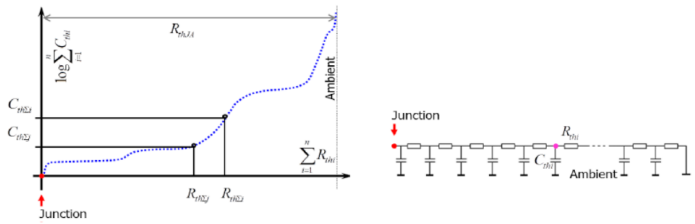

Figure 9. Structure function: the graphic representation of the thermal RC equivalent of the system

Steep sections of the function correspond to material regions of *high thermal conductivity*, because a huge amount of matter represents tiny additional thermal resistance only. These are typically metals; the steepness also may indicate large cross-sectional area. Sudden breaks in the slope indicate material or geometry changes.

Consequently:

- Thermal resistance and capacitance values of details in an assembly can be measured based on the temperature response on a single power step. In this way structure function methodology can be used for device characterization or failure analysis.
- When geometrical dimensions are known, heat transfer coefficients and specific heat values can be directly determined from the structure functions, either in-situ, in a real system or in its mock-up.
- Moreover, in instruments where the thickness of samples can be controlled or at least determined, thermal parameters of material layers or sheets can be measured, as the function of thickness and pressure.

Figure 10 shows the structure functions converted from the temperature transients of *Figure 1*. The internal layers of different quality can be observed, and also the flat plateau corresponding to the thermal paste after the divergence point at 0.75 K/W and 1.1 J/K.

In structure functions, many details of an actual assembly can be distinguished along with their partial thermal resistance and capacitance values. However, it should be noted that the structure function analysis is not a fully automated ("black box") technique.

There are three ways to assign actual assembly components to sections in the structure function. These are:

- The manufacturer of the device may know all internal geometries and material parameters. In such a way, a "synthetic" structure function can be built up by, for example, superposing slices of material with given thermal resistance and capacitance in a spreadsheet tool, and comparing the measured structure functions to it.
- An approximate model can be built up in a finite element or a finite difference simulation tool. Thermal transients can be simulated in the tool and structure functions can be composed of those. Geometry and material parameters can be fine-tuned until the simulated and measured structure functions match.
- Measured structure functions can be compared to an already identified "golden device". This technique is advantageous in production control.

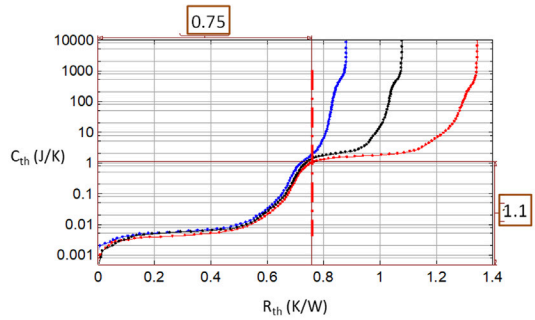

Figure 10. Structure functions of the three samples of the same manufacturing lot and the test bench

In this short overview of the origin of structure functions and their possible use in thermal transient measurements and simulations, we intended to draw the attention of thermal engineers to the growing importance of thermal transient testing. We hope that we succeeded to raise the awareness of the readers towards this very important method. Use cases and application fields can be found in the papers listed in the references and in other related publications of the authors.

REFERENCES

[1] https://en.wikipedia.org/wiki/Convolution, acessed 15-MAY-2021

[2] V.Szekely: "Identification of RC networks by deconvolution: Chances and Limits", IEEE Trans. On Circuits and Systems – I: Fundamental Theory and Applications, Vol.45, No.3, pp.244-258, 1998. DOI: 10.1109/81.662698

[3] JEDEC Standard JESD51-14, "Transient Dual Interface Test Method for the Measurement of Thermal Resistance Junction-to-Case of Semiconductor Devices with Heat Flow through a Single Path" (November 2010) Available online: http://www.jedec.org/sites/default/files/docs/JESD51-14_1.pdf (accessed on 13 January 2021).

[4] D. Schweitzer, H. Pape, L. Chen: "Transient Measurement of the Junction-To-Case Thermal Resistance Using Structure Functions: Chances and Limits", Proc. 24th SEMITHERM, San Jose, CA, 2008, DOI: 10.1109/STHERM.2008.4509389

[5] Katsuaki Suganuma (editor) : " Wide Bandgap Power Semiconductor Packaging", 1st Edition (Materials, Components, and Reliability), eBook ISBN: 9780081020951, Paperback ISBN: 9780081020944, Woodhead Publishing, May 2018

[6] P. Szabo; O. Steffens; M. Lenz; G. Farkas: "Transient junction-to-case thermal resistance measurement methodology of high accuracy and high repeatability", IEEE Trans. on Components and Packaging Technologies , 2005, Vol. 28, Issue: 4 pp: 630-636

Thermal Quality Assessment of Semiconductor Components

Voon Hon Wong, Diane DuVall, Andras Vass-Varnai
SIEMENS Digital Industry Software

Sujay Singh
ON Semiconductor

Márta Rencz
Budapest University of Technology and Economics

Voon Hon Wong
Hon Wong is the APAC Business Development Manager in the Mechanical Analysis Business Development Team, based in Singapore. He represents the Simcenter Flotherm and MicReD product lines. He has been using CFD tools for thermal and flow analyses in electronics for two decades and has worked on thermal management and design issues. He is also experienced in the Energy, Building and Process industries, etc. using CFD solutions. He was previously with Flomerics and Vestas prior to joining Mentor Graphics, a Siemens Business. He graduated from the University of London and holds a PhD. from Cranfield University.

Diane DuVall
Diane M. DuVall joined Siemens in 2018 as a Presales Industry Consultant for the semiconductor industry. Diane is a passionate advocate for semiconductor customers in realizing their success through digital transformation with Siemens products. Diane obtained a BS in Chemical Engineering from Pennsylvania State University and a MBA from Arizona State University. Diane began her career as a wafer process engineer moving to product engineering and then marketing and sales positions, and has over thirty years of industry experience with Motorola SPS, VLSI Technology, Rockwell Semiconductor, Conexant, Skyworks Solutions, and Jazz Semiconductor. Diane's background also includes experience with semiconductor test data analytics at Galaxy Semiconductor and Mentor Graphics, complementing her product engineering experience. Diane also gained experience in electronics while working for Navman Wireless, focusing on GPS solutions.

Andras Vass-Varnai
Andras Vass-Varnai obtained his MSc and PhD degrees in electrical engineering at the Budapest University of Technology and Economics. He started his professional career at the MicReD group of Mentor Graphics as an application engineer in 2007.Andras worked most for over 10 years as a product manager, supporting development projects, such as the DynTIM or the Powertester instruments. Before starting his current role as a global business development manager in Siemens, Andras worked out of Seoul, Korea, supporting the Asian business activities. He is working out of Chicago IL currently, with dedicated focus on the US market growth. His main topics of interest include thermal management of electric systems, advanced applications of thermal transient testing, characterization of TIM materials and reliability testing of high power semiconductor devices.

Sujay Singh
Sujay Singh received the Ph.D. degree in physics from The State University of New York at Buffalo, Buffalo, NY, USA, in 2016. Sujay started his career at Fairchild Semiconductor as a Thermal Characterization Reliability Engineer in 2015. He is currently a Senior Principal Reliability Engineer at ON Semiconductor. He is involved in the process, device, and packaging development teams to assess the thermal and mechanical properties and reliability of power semiconductors. His current research interests include electronic and thermal transport in micro/nanoscale, semiconductor device packaging, reliability, failure analysis, and resistive switching.

Márta Rencz
Márta Rencz received the Electrical Engineering degree, the Doctor in Engineering Degree and the PhD degree from the Budapest University of Technology and Economics. She has received the Doctor of Science degree from the Hungarian Academy of Science in the field of Microelectronics. She is a professor at the Budapest University of Technology and Economics. She has participated in numerous international research projects, mostly in the field of investigating, measuring and modeling multi-physical effects in electronics. She has published her theoretical and practical results in more than 300 technical papers. She was a co-founder and CEO of MicRed Ltd that is now part of Siemens DI, where she still holds a research director position.

INTRODUCTION

Reduction in early life failures and continuous quality improvements are "table stakes" for semiconductor manufacturers servicing the automotive industry. "Industry analysts expect that the automotive semiconductor market will be the fastest growing end use market for chips from 2017–21, with a 6.4 percent CAGR and a total market value of between $39-42 billion with conventional vehicles contain an average of $330 value of semiconductor content while hybrid electric vehicles can contain up to $1,000 and 3,500 semiconductors." [1] The global power electronics market size is projected to grow from USD 35.1 billion in 2020 to USD 44.2 billion by 2025, at a CAGR of 4.7%. [2] To satisfy the automotive quality standards to support this market growth, semiconductor companies are still challenged to achieve zero defects and continue to look for new ways towards this goal.

Historically, semiconductor companies would deploy early life failure reduction efforts with electrical testing or geospatial techniques to reject or test out potential failures. Burn-in and predictive test techniques like part average testing have been around for a long time. Additionally, other geospatial methods, such as visual defect screening and algorithmic yield clustering looking for abnormal patterns, are used to predict early life failures. In the quest for zero defects, companies must reduce defects and also reduce variability. As thermal metrics are one of the most important characteristics of a power electronics component, inline thermal resistance measures add another road to quality for semiconductor companies. Furthermore, the quality of the manufactured components heavily depends on the stability of process parameters which are not always simple to control.

As an example, the materials used in die attach compounds contain chemicals that are hygroscopic in nature. Moisture is absorbed from the environment when the material is exposed. Consequently, any temperature increase during the curing process can result in moisture evaporation that leads to voiding. The die attach pastes also contain volatile compounds which can outgas and cause voids with elevated temperatures. Voids can also arise from the thawing of the die attach paste. The pastes are typically stored in plastic syringes at -40°C. During the thawing process prior to the application of the pastes, there is a difference in the coefficient of thermal expansion between the plastic and paste, which can trap pockets of air at the interface between the two different materials. This can then lead to voids when the paste is applied.

The presence of voids in die attach joints can lead to the development of cracks and interfacial delaminations. If the packages are subjected to a reflow process, any absorbed moisture will vaporize, resulting in higher stress concentrations and the formation of cracks. Interfacial delaminations are caused by voids near or at the interfaces. The presence of these voids reduces the adhesion between the two surfaces, and potentially leading to failure.

Besides the adverse effects on the mechanical strength of the packages, the presence of these defects in the die attach layer will increase the overall thermal resistance of the package, and hence negatively affect the junction temperatures of these devices. The lifetime and reliability will be reduced accordingly.

We can quantify this using the power semiconductor example in *Figure 1*. The lifetime curve for this device operating at the maximum junction temperature is shown. The typical and maximum junction to case thermal resistances of the device vary between 0.14-0.17K/W. Using an average value of 0.15K/W for illustration purposes, a small increase of 5% in the thermal resistance due to the presence of voids, will give a value of 0.1575K/W. This will increase the junction temperature by just under 14°C. The number of cycles to failure is reduced from 26 million down to 1.6 million – corresponding to a tenfold reduction in the expected lifetime of the device.

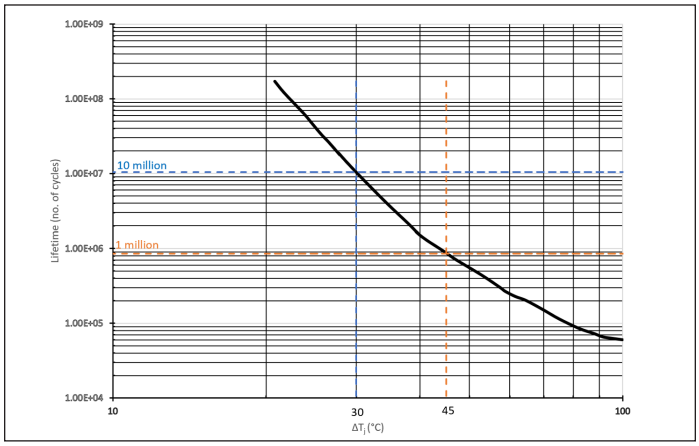

Figure 1. Thermal resistance variation impact shown on a lifetime curve for a power semiconductor device

Thermal Quality Test Process

In contrast to the visual identification of die attach voids, transient thermal testing can be used to detect the presence of any defects [3]. The tester communicates with an external handler, a robotic arm in our example, to pick up the components, place them onto the test jig, and bin them after the automatic evaluation is completed. This processes cycles continuously until all samples are evaluated and binned.

During the actual device test, a short heating pulse is supplied to the die and then turned off. This is followed by a brief cooling period where the temperature data is captured (*Figure 3*). The heating and cooling times will vary according to the design and internal layout of the packages to be tested, but typically, these will be in the order of maximum a few hundred milliseconds. This is sufficient to detect any defects within the structure. Consequently, the total testing time for a device, including the time for the external handler to position the device onto the test jig and bin it afterwards, would be on the order of seconds, at most. Hence the test throughput for this would be extremely high, and it will be possible to test every single component after the assembly process.

In a production environment, it is not necessary to carry out a full thermal characterization test for every single component. A shortened testing time that is able to sense the thermal response of the defective layer will be sufficient. Based on the theory established by Prof. Szekely, the mimimum heating time required to resolve the layer is one order of magnitude longer than its time constant. [4]

A process for implementing and improving thermal quality testing is shown in *Figure 4*. This involves an initial thermal characterization test of a golden reference device (good sample without any defects). The results from this test is used as the reference for comparisons with the other samples to be tested.

Additionally, the structure function curve for the golden reference is used to calibrate a thermal simulation model created using commercially available software [5]. An accurate thermal simulation model is useful for investigating the presence of voids and to quantify how the overall thermal resistance of the packages will change with respect to the void size variation. Ultimately, the results from the void tests can be used to set the binning criteria for the tester.

The thermal quality tests can begin once all the previous steps are completed. The flowchart in *Figure 4*, includes a fourth step marked in yellow. This represents a potential approach in which the collected test data are used to finetune the binning criteria by overriding the recipe files that define the test conditions.

Initially, the binning criteria is manually set by the operator (*Figure 5*). Multiple bins can be defined, and the minimum and maximum thermal resistance values are specified at different time

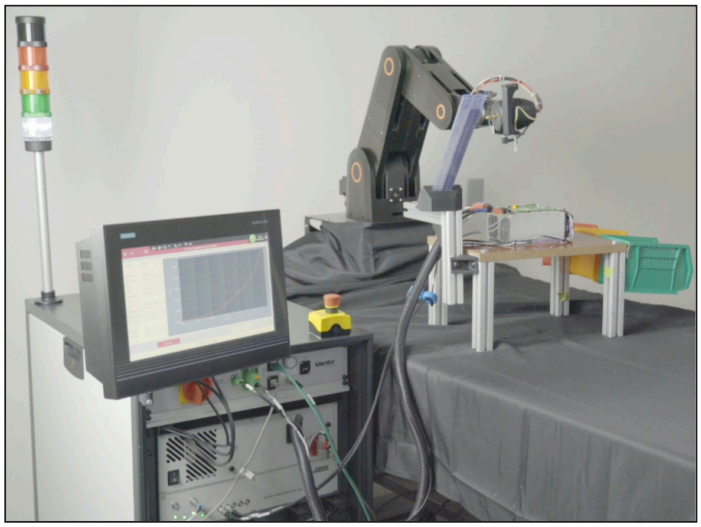

Figure 2. Tester with optional robotic arm

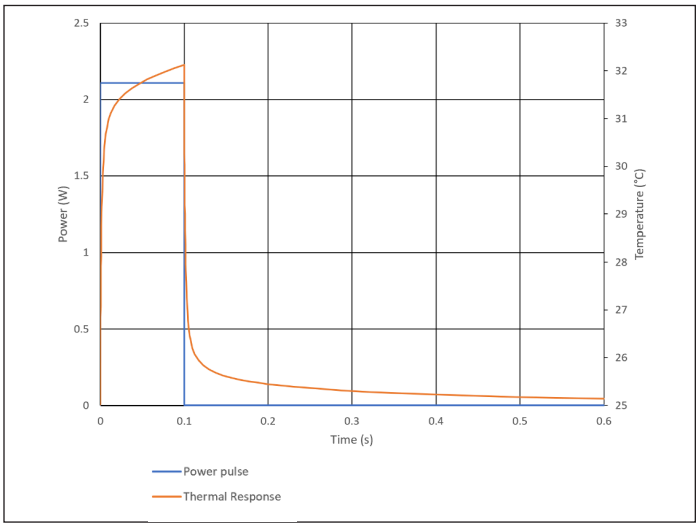

Figure 3. Reduced heating and cooling times for thermal quality tests

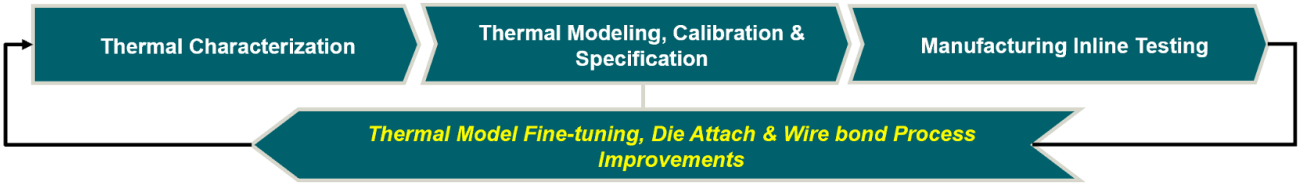

Figure 4. Thermal quality test workflow

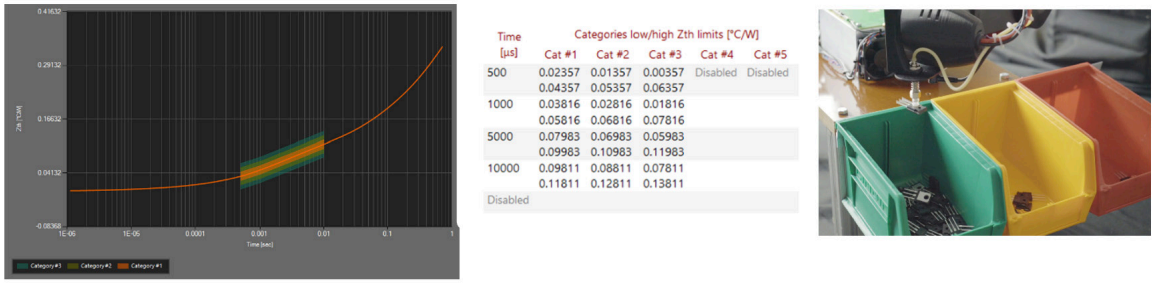

Time [µs]	Categories low/high Zth limits [°C/W]				
	Cat #1	Cat #2	Cat #3	Cat #4	Cat #5
500	0.02357	0.01357	0.00357	Disabled	Disabled
	0.04357	0.05357	0.06357		
1000	0.03816	0.02816	0.01816		
	0.05816	0.06816	0.07816		
5000	0.07983	0.06983	0.05983		
	0.09983	0.10983	0.11983		
10000	0.09811	0.08811	0.07811		
	0.11811	0.12811	0.13811		
Disabled					

Figure 5. User defined binning criteria. Three bins are created – good (green), medium (yellow), and poor (red)

intervals. These bands are displayed graphically in the software.

Devices whose measured thermal resistances fall within the preset, defined bands will be placed in the correct bin automatically by the test handler. The implementation of different bins can improve the production yield by reducing the number of faulty components in assemblies.

Identifying Binning Criteria

Thermal simulations using of a TO-220 device were carried out (*Figure 6*). The objectives for these tests were to determine the suitable measurement times for this device, quantify the thermal effects of die attach voids and also to use the simulation results to determine the binning criteria.

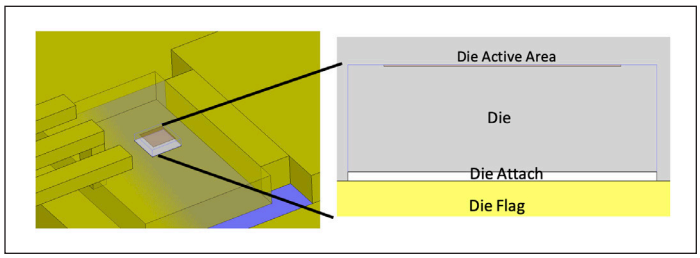

Figure 6. TO-220 MOSFET structure used in the thermal simulations

This device was measured previously with a transient thermal tester [6] and the test results were used to calibrate the simulation model prior to any die attach void investigations. *Figure 7* shows the results of this automated calibration exercise. With a calibrated thermal model, we would be confident of the accuracy of the thermal and transient response of this device for our subsequent investigations.

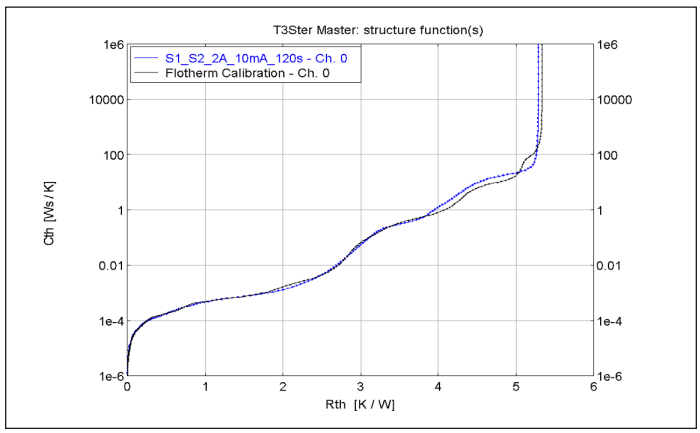

Figure 7. Thermal model calibration result

Voids within the die attach layer of the package were then simulated through the use of cuboid blocks, as seen in *Figure 8*.

Different void sizes were modelled, ranging from 1.34% to 65.71% by volume and resultant thermal impedance curves are shown in *Figure 9*. The larger the void size, the higher the temperature elevation.

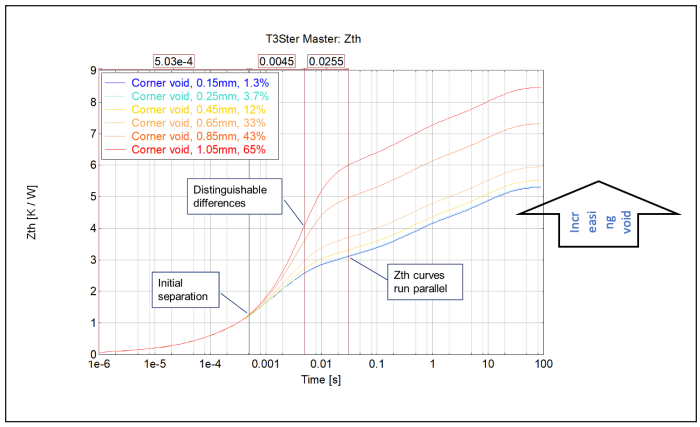

Figure 9. Thermal Impedance curves of the corner void simulations

Thermal impedance curves are suitable to observe the effects of voids in the model, structure functions can later help to analyze the exact location of the void. The thermal impedance curves can also be used to estimate the required measurement times. In this case, we see that the curves begin to diverge at around 0.5 ms. At 5ms, we are already able to distinguish the differences between most of the cases. By around 30 ms and beyond, the thermal impedance curves become parallel to one another. By delaying the measurement time to 50 ms, we would ensure that heat flow path within the package has travelled to the die attach and beyond. Visually, it is possible to view the differences in thermal resistance or thermal impedance for all the different void size cases. The only two exceptions are the two initial cases with void sizes of 1.34% and 3.72%. The curves for both lie very close to the no defect case. This indicates the lower limit of the detectable void sizes on thermal impedance for this device under test.

We are able to visualize the heat flow path within the package by plotting the heat flux vectors developed at 50ms, as shown in *Figure 10*. The heat travels down towards the heatsink upon which the device is mounted on. It then spreads out in a conical fashion towards the other structural layers within the device.

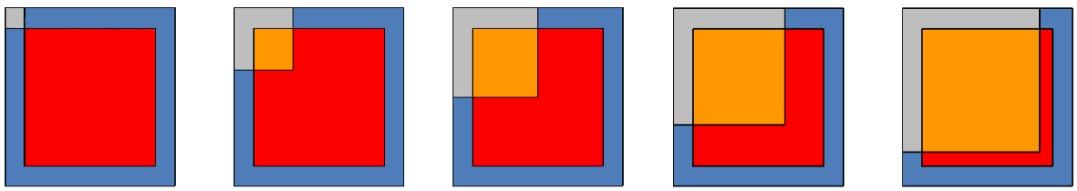

Figure 8. Simulated voids emanating from the top left corner of the die attach

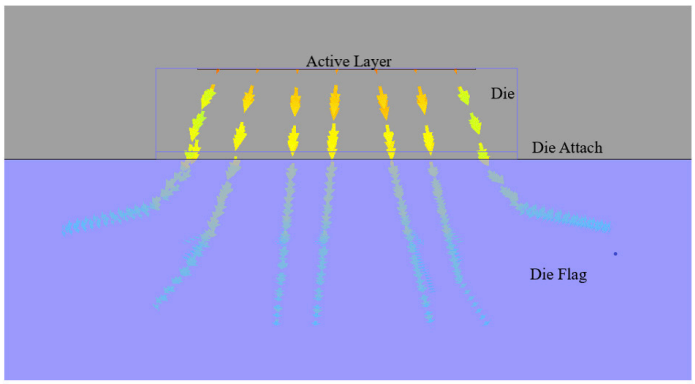

Figure 10. Heat flux vectors developed within the TO-220 package

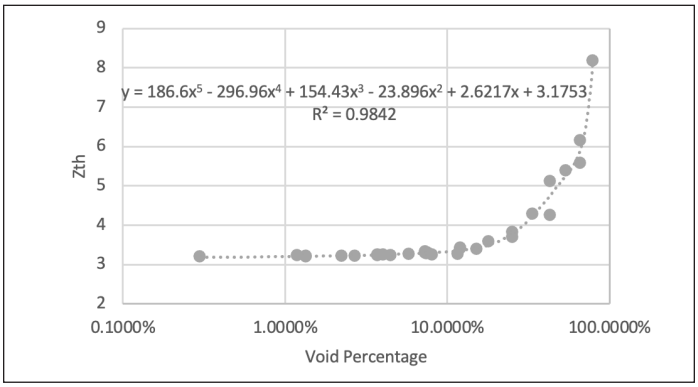

Figure 11. Thermal Impedance and void size relationship for a TO-220, and the binning criteria

Void Volume (%)	Z_{th} @ 0.05s (K/W)	Increase in thermal impedance (ΔZ_{th}) (%)	Binning Criteria
0	3.18	0.0	Good
0.50	3.19	0.39	Good
1	3.20	0.76	Good
3	3.24	1.92	Good
5	3.26	2.80	Good
7	3.29	3.55	Good
9	3.31	4.30	Medium
10	3.33	4.72	Medium
15	3.42	7.58	Medium
20	3.56	12.24	Poor
40	4.59	44.64	Poor

Table 1. Binning criteria based on simulation results

Besides the corner voids, other scenarios with voids in the centre of the die, different numbers of voids and different shapes of the voids, were also considered. These tests, summarized in *Figure 12*, show an increasing thermal impedance (Z_{th}) values with greater void sizes. A polynomial curve fit can be constructed to quantify this relationship between the two variables. From this relationship, we can calculate the thermal impedance values at a specific time corresponding to the measurements. From there, we use the percentage increase in thermal impedance as the criteria for binning. In this example, any samples with a $\Delta Z_{th} < 4\%$ will go to the 'Good' quality bin. The 'Medium' quality bin is $4\% < \Delta Z_{th} < 15\%$. Samples with $\Delta Z_{th} \geq 15\%$, will go to the 'Poor' quality bin. *Table 1* shows examples of this.

In conclusion, a transient thermal tester is capable of quickly detecting the presence of defects within the package thermal structure with non-destructive testing. The method equally works with assemblies, but the required heating and cooling times increase accordingly. All measurements are compared to data collected from a reference sample, in the thermal impedance space. Binning criteria can be easily defined, either based on simulation experiments or real physical tests.

Binning criterion would help define the absolute maximum ratings of the components. Components that would be rejected using stringent yield criteria could now be used for less demanding performance requirements. Binning based on this thermal metric would allow widening of the product portfolios for various applications and markets.

The ability to test every single component in production is a key advantage in power electronics as component manufacturers can reduce infant mortality of their components, track component thermal information and meet increasingly stringent quality and reliability requirements demanded by the current vehicle electrification megatrend.

REFERENCES

[1]https://www.usitc.gov/publications/332/executive_briefings/ebot_amanda_lawrence_john_verwey_the_automotive_semiconductor_market_pdf.pdf

[2] https://www.marketsandmarkets.com/Market-Reports/power-electronics-market-204729766.html?gclid=Cj0KCQjwvYSEBhDjARIsAJMn0lggEHgHsasGccQXgLPKmlFnJ2p8iQMEDg-7Gzifw3PCBuC9eN3BYQOgaAmODEALw_wcB

[3] SimcenterTM MicredTM Thermal Quality Tester - https://www.plm.automation.siemens.com/global/en/products/simcenter/micred-quality-tester.html (last visited on the 28th of May, 2021)

[4] V. Székely, "Evaluation of short pulse and short time thermal transient measurements", Microelectronics Journal, Volume 41, Issue 9, 2010, Pages 560-565

[5] Simcenter FlothermTM - https://www.plm.automation.siemens.com/global/en/products/simcenter/flotherm.html (last visited on the 28th of May, 2021)

[6] Simcenter Micred T3STER - https://www.plm.automation.siemens.com/global/en/products/simcenter/t3ster.html (last visited on the 28th of May, 2021)

Emerging 5G Networks: Potential Economic Benefits of Two-phase Thermal Management

Raffaele Luca Amalfi[1], Ryan Enright[1], Vasileios Kafantaris[2]
[1]Nokia Bell Labs, Thermal Management Research, Efficient Energy Transfer Dept., Murray Hill, NJ, USA
[2]Nokia Mobile Networks, Deploy Services, Site Engineering Department, Athens, Greece

Last modification: April 20, 2021

CONTEXT

The fourth and future industrial revolutions will set new requirements for smart cities / factories, autonomous vehicles, augmented reality, smartphones, etc., resulting in more distributed architectures, expanding the convergence of new technologies and developments thus, transforming the term Internet of Things (IoT) to Internet of Everything (IoE). Centralized cloud computing has evolved to provide scalable computation capable of processing large amounts of data, while also ensuring storage and provisioning of resources according to user requirements. The explosion of cloud- and internet-based content has created new business opportunities with a natural "shift to the edge" closer to where the users are, in order to meet bandwidth requirements and to deliver faster services with minimal latency, the latter being fundamentally limited by the propagation speed of light in optical fibers. These demands, in turn, create a tremendous need for distributed datacenters where some portion of the compute function is shifted from the

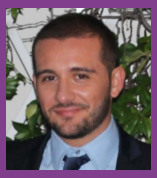

Raffaele Luca Amalfi
Raffaele Luca Amalfi is a Senior Lead Researcher at Nokia Bell Labs New Jersey in the Efficient Energy Transfer (ηET) Department, where he performs cutting-edge research in the field of thermal management of high-performance communications and computing systems across multiple scales. He is the Principal Investigator on behalf of Nokia of America Corporation and Bell Labs for the Eurostars Project PCOOLDATA focused on the development of innovative cooling solutions for datacenters. Since 2016 he worked as Scientific Collaborator and Lab Manager at the Swiss Federal Institute of Technology of Lausanne (EPFL), at the Heat and Mass Transfer Lab, in Switzerland. In 2015 he joined Alcatel-Lucent Bell Labs in New Jersey, where he performed disruptive research on hybrid cooling technologies for telecom equipment. In 2012 he joined IBM Research Lab in Switzerland where he developed a novel cooling system for high-power electronics. He has received a Ph.D. in Energy Engineering from the Swiss Federal Institute of Technology of Lausanne and authored over 38 scientific publications in leading journals, conference proceedings and handbooks. He is a Member of the ASME K-16 Heat Transfer Committee, Guest Editor for the ASME Journal of Electronic Packaging, and is the recipient of the Best Paper Award at IEEE / ITHERM 2020 and the Outstanding Paper Award at ASME / InterPACK 2017.

Ryan Enright
Ryan Enright is a Member of Technical Staff at Nokia Bell Labs New Jersey in the Efficient Energy Transfer (ηET) Department, where his research spans the areas of materials interface engineering, micro/nanoscale heat/mass transfer, passive heat transfer mechanisms and integrated RF, photonic and electronic thermal management. He was the Nokia Bell Labs PI on the EU H2020 Thermally Integrated Smart Photonic System (TIPS) project (2014-2018) and is currently a co-PI for the EU Eurostars PCOOLDATA project. He received his B.Eng.(Hons) and PhD. degrees in Mechanical Engineering from the University of Limerick, Ireland in 2004 and 2008, respectively. He was a Research Assistant at Bell Labs (USA) from 2005-2007 during his doctoral work. After receiving his PhD., he was a SFI CTVR postdoctoral associate from 2008-2009 and a Marie-Curie postdoctoral fellow at the Massachusetts Institute of Technology from 2009-2012. He was a Senior Member of Technical Staff in the Efficient Energy Transfer (ηET) Department at Nokia Bell Labs Dublin (2012 -2020) before relocating to Nokia Bell Labs New Jersey.

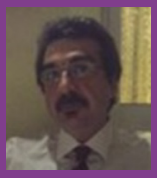

Vasileios Kafantaris
Vasileios Kafantaris is a Project Manager at Nokia Mobile Networks Athens, Greece, responsible for datacenter deployment projects of Nokia. He holds two degrees in Mechanical & Electrical Engineering. Having more than thirty years of experience, he has been designing and deploying full turnkey datacenters (new or upgrade) and / or Business Critical Continuity (BCC) related installations in different countries and market segments including banking, information technology (IT), telecommunications and private sector.

centralized cloud. The "shift to the edge" represents the most profound change in the network architectures that will impact for decades to come. The importance of edge computing to 5G radio access network (RAN) infrastructure is expected to kick off with enhanced mobile broadband as its first use case. Data scientists have predicted that by the end of 2025, there will be 2.8 billion 5G subscriptions, compared to about 190 million in 2020 [1, 2].

Emerging 5G networks are expected to have a service-based architecture, meaning that network functions can be delivered as service components with the implementation of edge computing on cloud-based hardware. In this context, 5G will become a major demand driver for distributed datacenters, which will be used to enhance network capabilities of an increased number of radio access points. It has been reported that the global edge computer hardware represents a potential value of $175 billion to $215 billion by 2025 [3]. Further forecasts show that over $700 billion in cumulative Capital Expense (CAPEX) will be spent within the next decade on edge information technology (IT) infrastructure and data center facilities including edge equipment at access network sites, e.g., radio base station tower sites (*see Figure 1*), pre-aggregation sites, e.g., street-side cabinets, and aggregation and central office sites rearchitected as data centers [4, 5]. In this context, major physical deployment challenges for edge datacenters can be summarized as follows:

- Enabling quick and volume scaling in order to meet the demands of dynamic cloud-based services;
- Increasing hardware densification, quantified as kW/m^3, while reducing capital and operating expenses;
- Deploying energy efficient and eco-friendly installations, requiring minimal supporting infrastructure;
- Providing hardware platforms that are simple, reliable and easily maintainable, i.e., good serviceability.

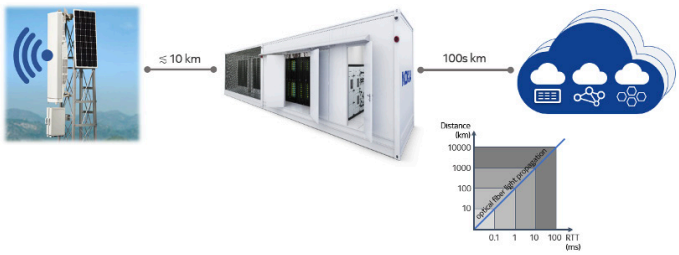

Figure 1. Example of a cloud RAN architecture. The mobile base station (left) is connected by optical fiber to a closely located containerized edge datacenter (middle) that may handle radio processing aggregation and/or compute for low-latency service delivery. Non-latency critical traffic is sent to the centralized cloud compute (right) via the optical network. The architecture is fundamentally driven by the finite propagation speed of light along an optical fiber as indicated by the diagram in the lower right.

The most recent survey proposed by the Uptime Institute has indicated an average Power Usage Effectiveness (PUE) of 1.59 in 2020 across 1100 datacenters worldwide [6]. This implies that the IT energy consumption portion is ≈ 63% and non-IT energy consumption portion (thermal management solution, lights, equipment losses, etc.) is ≈ 37%. Our internal studies indicate that lighting, uninterruptible power supply system and other facilities losses typically do not exceed ~5% of the total energy budget; therefore the average thermal management energy consumption is ≈ 32%. The latter can be higher as mentioned in the same Uptime Institute report: "…there are still thousands of older datacenters that cannot be economically or safely upgraded to become energy efficient…", including the ones to be re-used in the edge network architectures, e.g., CORD (Central Office Re-architected as a Datacenter). These results, combined with the massive grow of edge compute, necessitates a paradigm shift in the thermal management solution to support emerging 5G networks. The next two sections provide an overview of the proposed thermal management solution, including a discussion on the performance metrics, and a Total Cost of Ownership (TCO) analysis for a specific 5G use case, namely a containerized data center deployment, highlighting the business benefits.

TWO-PHASE THERMAL MANAGEMENT SOLUTION

Passive two-phase cooling represents a viable and long-term solution for efficient cooling of datacenters, achieving high-performance and reliability [7]. The proposed technology leverages several two-phase heat sink implementations, e.g., cold plate evaporators, low-height thermosyphons, thermo-heat pipes, etc., to dissipate the heat generated by the critical components inside the servers. Then, the heat is transferred to multiple rack-level thermosyphons, equipped with an overhead compact heat exchanger that dissipates the total heat from the rack into the room-level cooling loop. A schematic of the technology is reported in *Figure 2A*, while close-up views of the server-level heat sinks are shown in *Figures 2B* and *2C*.

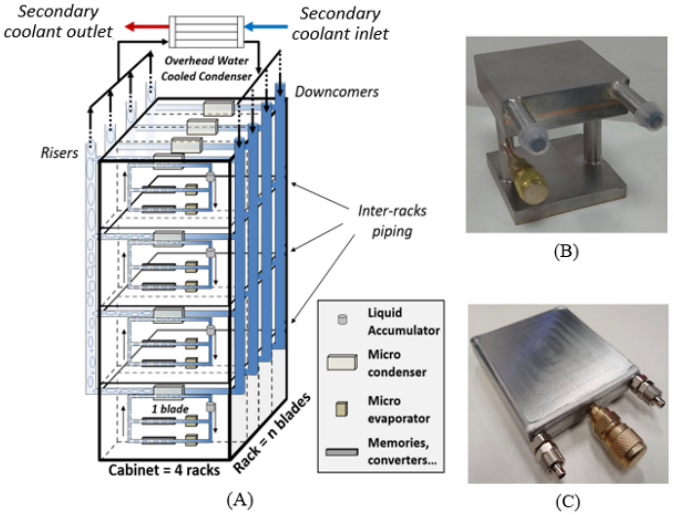

Figure 2. Passive thermal management solution for next-generation high-performance datacenters. (A) Rack-level thermosyphon architecture to transport heat from the servers to a heat exchanger at the periphery of the rack. Examples of server-level two-phase heat sinks: (B) a thermosyphon with a minimum thermal resistance of ≈ 0.085 K/W; (C) a thermo-heat pipe with a minimum thermal resistance of ≈ 0.065 K/W.

The system level advantages of this thermal management approach include passive thermal energy transport to the rack edge, high thermal performance obviating the needs for active cooling at the room-level, e.g., air-conditioning, under European Telecommunications Standard Institute (ETSI) and Network Equipment Building System (NEBS) deployment environments and the use of reliable two-phase heat sinks. The performance data of the heat sink prototypes shown in *Figures 2B* and *2C* can be found in Amalfi et al. [8] and Cataldo et al. [9].

CASE STUDY: BUSINESS BENEFIT OF ADVANCDED THERMAL MANAGEMENT OF EDGE COMPUTE IN 5G NETWORKS

Radio access networks (RAN) consume significant amounts of energy and, despite massive improvements in efficiency in terms of J/bit, this is expected to grow in the 5G era. Important 5G radio architectures, including multi-band remote radio heads (RRH) and massive Multiple Input Multiple Output (MIMO) active antennas, coupled with edge datacenters for radio processing aggregation and low-latency compute capability will be key features in these advanced RAN. In principle, passive two-phase cooling could be applied to efficiently cool multiple sub-systems across the 5G RAN. However the main focus of this section is to investigate the impact of the thermal management solution for a containerized edge compute deployment, including a TCO analysis to highlight the potential economic benefits.

Air-based cooling coupled with in-row air-conditioning units is compared to passive two-phase cooling in a TCO analysis for a containerized edge datacenter considering the specifications listed in *Table 1*. In addition, *Table 2* presents the case where the datacenter is reduced in size with a more densified IT hardware deployment, enabled by the use of the passive two-phase cooling technology (higher power servers and footprint reduction). The TCO analysis incorporates site infrastructure costs, IT capital costs, operating expenses and energy costs informed by historical deployment projects.

Table 1. Traditional datacenter (edge compute) specifications.

PARAMETER	VALUE
Number of racks	2
Number of servers per rack	47
Power use per server	532 (W)
Power use per rack	≈ 25000 (W)
Total power / IT load	≈ 50000 (W)
Datacenter footprint	≈ 15 (m^2)

Table 2. Densified datacenter (edge compute) specifications.

PARAMETER	VALUE
Number of racks	1
Number of servers per rack	36
Power use per server	1389 (W)
Power use per rack	≈ 50000 (W)
Total power / IT load	≈ 50000 (W)
Datacenter footprint	≈ 9 (m^2)

The layouts of the three deployment scenarios are illustrated in *Figure 3*. The baseline air-cooled edge datacenter (see *Figure 3A*) uses four in-row air-conditioning units for room-level cooling. The passive two-phase cooled edge datacenters (see *Figure 3B* and *3C*) incorporate two dry-coolers and two ventilation fans for room-level cooling. The cost estimates of the subsystems, such as in-row cooling units, dry coolers, etc., are based on market available data. The hardware costs of servers and racks, between in-row air cooling and passive two-phase cooling solutions, take into account the additional expenses associated with quick couplings, inter-rack piping, server-level heat sinks (see *Figures 2B* and 2C), overhead heat exchanger (see *Figure 2A*) and refrigerant charge.

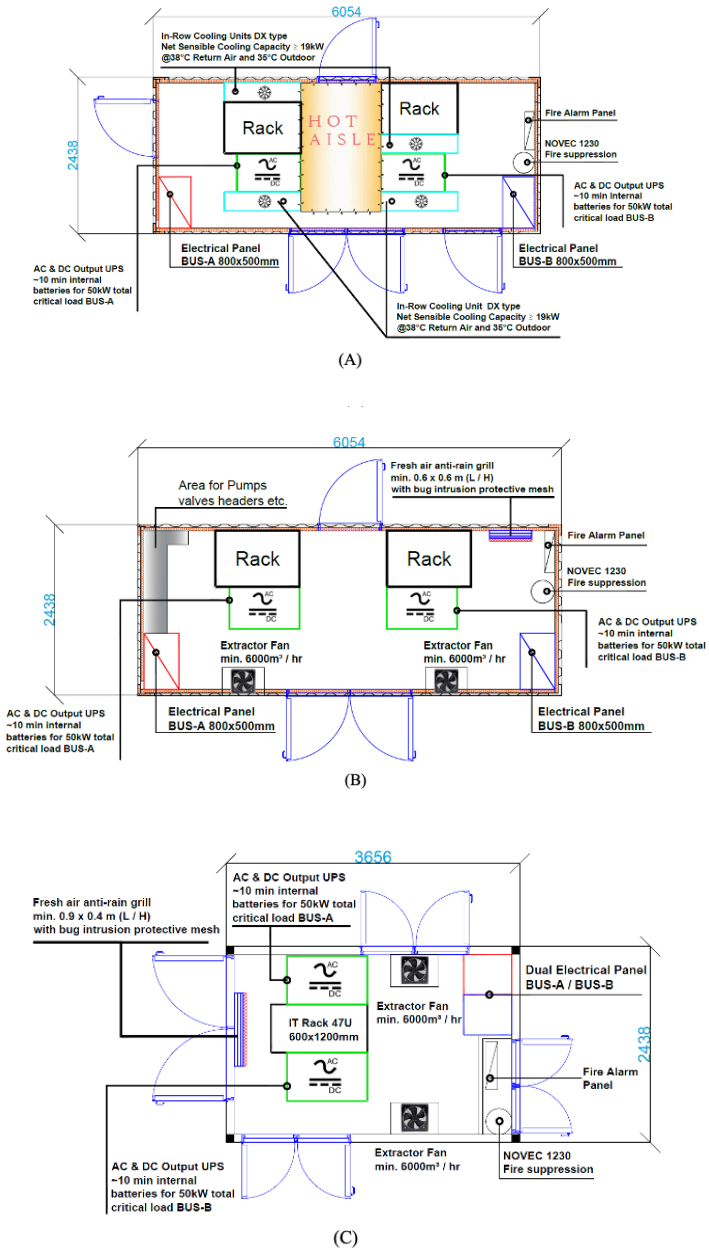

Figure 3. Deployment scenarios of a far-edge datacenter: (A) in-row air-based cooling with standard servers; (B) two-phase cooling with standard servers; (C) two-phase cooling with densified servers.

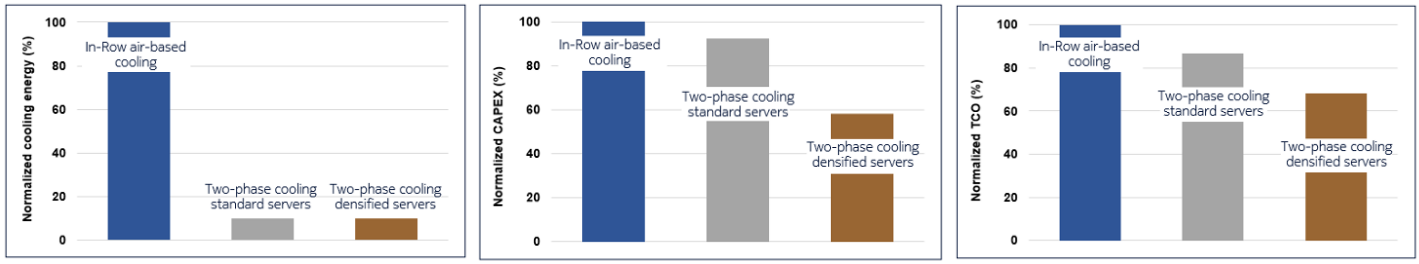

Figure 4. Summary of the results considering the three deployment scenarios introduced earlier: (A) normalized cooling energy per year; (B) normalized CAPEX per year; (C) normalized TCO per year.

The economic benefits identified in the TCO analysis are discussed based on three figures of merits reported in *Figure 4*: the cooling energy, CAPEX, and TCO, which are all normalized with respect to the reference deployment scenario of in-row air-based cooling. There are significant energy savings when switching from in-row air cooling to passive two-phase cooling due to the passive thermosyphon nature, coupled with a more efficient cooling approach at room-level. PUE calculations for the two cases show a reduction from 1.38 to 1.08, where the cooling energy portion represents 24% and 3% of the total energy cost, respectively. CAPEX is reduced when going from air-based cooling to passive two-phase cooling with standard servers, mainly due to the cost savings of the in-row units. A more significant CAPEX reduction can be achieved when the datacenter is deployed with passive two-phase cooling and densified servers due to the additional savings in the IT capital costs. This translates into a projected 32% TCO reduction for densified servers that is enabled by passive two-phase cooling in comparison to the baseline air-based cooling case, where it is assumed that the server cost per Watt is reduced by ≈ 50%.

Finally, the three deployment scenarios of a far-edge datacenter, including in-row air-based cooling, two-phase cooling with standard servers and two-phase cooling with densified servers, are compared using an overall Figure of Merit (FoM) as reported in *Figure 5*. The FoM proposed here takes into account the IT load as a function of datacenter size, energy efficiency and datacenter deployment cost:

$$FoM = \frac{P_{IT}}{V_{DC}}\left(PUE \cdot CAPEX^{*}\right)^{-1}$$

where PIT is the IT load (W), VDC is the overall datacenter volume (m^3) and CAPEX* is the datacenter deployment cost normalized to the reference air-cooling deployment cost case (-), as reported in *Figure 4B*. The FoM favors low-cost, energy-efficient and dense IT deployments. Thus, the FoM increases when a far-edge datacenter is deployed with two-phase cooling, and in particular, the highest FoM is found for two-phase cooling with densified servers as the power density is maximized, while optimizing PUE and providing a reduced CAPEX.

CONCLUSIONS

Emerging 5G networks will enable new use cases and drive a services delivery model for the telecommunications industry. The need for reduced latency to deliver these new use cases, and an increased density of radio access points, requires the deployment of edge compute to aggregate radio processing and shift some workloads from the cloud. Edge compute must be deployed in a way that maximizes energy efficiency and minimizes cost to establish the business case and achieve critical sustainability goals. Two-phase cooling applied at the edge is projected to deliver efficiencies rivaling highly optimized hyper scale data center deployments at costs significantly lower than those achieved in the current air-cooling paradigm.

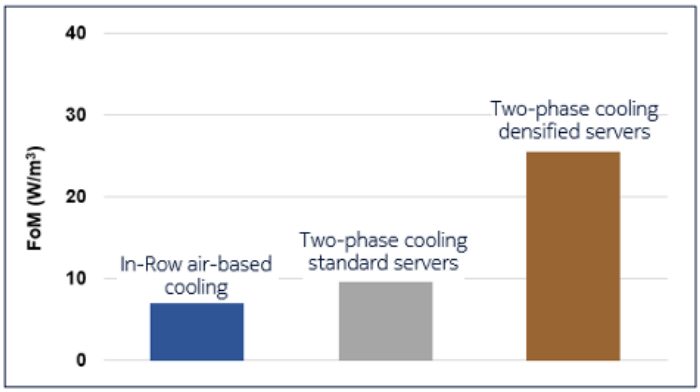

Figure 5. Proposed FoM for the three deployment scenarios considered in this study.

REFERENCES

[1] M. Bourke, Working in More-than-Moore, Lam blog on technology, Lam Research, October 2019, (https://blog.lamresearch.com/working-in-more-than-moore/), [Accessed December 2020].

[2] G. Sharma, Big data & cloud computing: the roles & relationships, IEEE Computer Society, Publications/Tech News/Trends, 2020, (https://computer.org/publications/tech-news/trends/big-data-and-cloud-computing), [Accessed January 2021].

[3] J.M. Chabas, C. Gnanasambandam, S. Gupte, M. Mahdavian, New demand, new markets: What edge computing means for hardware companies, McKinsey & Company, November

2018, (https://mckinsey.com/industries/technology-media-and-telecommunications/our-insights/new-demand-new-markets-what-edge-computing-means-for-hardware-companies#), [Accessed November 2020].
[4] M. Trifiro, J. Smith, About State of the EDGE report, The Linux Foundation Projects, 2020 (https://stateoftheedge.com/about/), [Accessed January 2021].
[5] Technical Steering Team (TST), Central Office Re-architected as a Datacenter (CORD), Open Networking Foundation (ONF), (https://opennetworking.org/cord/), [Accessed December 2020].
[6] R. Bashroush, A. Lawrence, Beyond PUE: tackling IT's wasted terawatts, Uptime Institute Survey, April 2020, (https://journal.uptimeinstitute.com/). [Accessed October 2020].
[7] R.L. Amalfi, F. Cataldo, J.R. Thome, The Future of Datacenter Cooling: Passive Two-Phase Cooling, Electronics Cooling Online Journal, Section of Data Centers, Free Air Cooling and Liquid Cooling, May 2020.
[8] R.L. Amalfi, F. Faraldo, T. Salamon, R. Enright, F. Cataldo, J.B. Marcinichen, J.R. Thome, Hybrid two-phase cooling technology for next-generation servers: thermal performance analysis, IEEE Intersociety Conference on Thermal and Thermo-mechanical Phenomena in Electronic Systems (ITHERM), 2021.
[9] F. Cataldo, Y.C. Crea, R.L. Amalfi, J.B. Marcinichen, J.R. Thome, Novel pulsating heat pipe for high density power data centres: performance and flow regime analysis, IEEE Intersociety Conference on Thermal and Thermo-mechanical Phenomena in Electronic Systems (ITHERM), 2021.

Upper Air Room Disinfection with UV-C Luminaire – Metrics and Multi-Domain Modeling Approach

Genevieve Martin, Marc van der Schans, Martin Creusen
Signify

In my editorial of Spring 2021, I questioned How our simulation community of experts can contribute in this pandemic time? I am coming back to present examples of contributions. While the general topic of this article is outside the typical scope of Electronics Cooling Magazine, it does illustrate how analysis methods that are discussed here, such as computational fluid dynamics, and technologies that are part of our industry, such as lighting, can be applied to address a problem that is both significant and timely to the entire world.

FACTS AND FIGURES

Since April 2020, already 3.3 million people have died of COVID-19 as recorded by Johns Hopkins university [1]. Worldwide, entities including research institutes, public health organizations, and national governments have been working for months to reduce the impact of the pandemic. Many measures, such as social distancing, using personal protective equipment, improving the safety of public spaces through proper ventilation, and developing vaccinations to ultimately achieve herd immunity have been implemented. This article describes a less well recognized, but important tool available for improving safety: upper room ultraviolet germicidal irradiation (UVGI) disinfection. On February 25th, 2021, the Center for Global Health Delivery, Advance Access & Delivery, the Belfer Center's Middle East Initiative at the Harvard Kennedy School, and Harvard Global Health Institute, hosted a webinar featuring a panel of engineers and infectious disease experts to talk about the safety and evidence base supporting the use of UR-GUV [2], [3].

This article discusses the concept of using ultraviolet light (UV-C) for disinfecting upper air, i.e., creating a disinfection zone near the ceiling of a room to avoid direct exposure of people to any dangerous UV radiation. It begins by describing the basics of UV, the airborne transmission route of SARS-CoV-2 and then

Genevieve Martin
Genevieve Martin (F) is R&D manager for thermal & mechanics competence at Signify (former Philips Lighting), The Netherlands. She is working in the field of cooling of electronics and thermal management for over twenty years in different application fields. She is currently leading the activities around modeling upper air disinfection in the context of COVID pandemic.

Marc van der Schans
Marc van der Schans is a Research Scientist in the Thermal & Mechanics group at Signify research, The Netherlands. In this role his main responsibilities include the development of solutions and knowledge relevant for thermal management of lighting products. Prior to joining Signify in 2019, he obtained a BSc, MSc and PhD degree in Applied Physics from the Eindhoven University of Technology, The Netherlands.

Martin Creusen
Martin Creusen is a Standards and Regulation (S&R) manager at Signify in the Netherlands. In this role, he is responsible for developing new performance standards for the evolving field of UV-C air disinfection, a key mitigation tool in the battle against airborne diseases. He received his M.Sc. degree in Applied Physics in 1994 and his PDEng degree in 1996 at the Eindhoven University of Technology.

explains how UV-C can disinfect the air. Finally, an example of how multi-domain simulation is used to assess the challenges, as well as the advantages of this approach, is presented.

UV-C HAS A LONG HISTORY AND TRACK RECORD IN EFFECTIVE DISINFECTION

UV-C is a well-established method for disinfection. UV-C light is a category of ultraviolet light with wavelengths between 100-280 nanometres (nm) and is the most effective UV light for disinfection. It has been applied ever since it was discovered to be an effective tool in preventing the spread of contagious diseases by disinfecting water, surfaces and air in very short time periods. UV-C light inactivates viruses and microorganisms such as bacteria, molds, spores, fungi and yeasts by destroying their DNA or RNA. It is generated by lamps, using well-known technology. Additionally, it is sustainable and more environmentally friendly than several other disinfecting means, e.g. chemical.

The first observation that microorganisms respond to light was published by Ludwig Karl Schmarda in 1845 [4]. The germicidal effect of ultraviolet light was discovered by Downes and Blunt in 1877 [5]. When they placed solution-filled test tubes outdoors, they discovered that sunlight could kill and inhibit the development of pathogenic bacteria. In 1935, Wells [6] demonstrated that UV-C, which had been used to kill microorganisms on surfaces and in liquids, could also be used to kill airborne infectious organisms. In the late 1950s and early 1960s, Riley et al. [7] [8] conducted a series of animal experiments that conclusively showed that intense ultraviolet germicidal irradiation (UVGI) in air ducts inactivates virulent M. tuberculosis in droplet nuclei. In 1975, Riley et al. aerosolized Bacillus Calmette-Guérin (BCG) into a test room and measured its inactivation with and without upper-room UV-C. They found a sixfold increase in the inactivation rate in the rooms that had upper-room UV-C installed [9]. In the late 1980s, there was a renewed interest in UV-C due to the unexpected rise in tuberculosis (TB) and the emergence of multiple drug-resistant strains. In 2009, Escombe et al., [10] published a clinical trial using upper-room UV-C as an effective, low-cost intervention to prevent TB transmission in high-risk clinical settings. Mphaphlele's paper [11] in 2015 showed that upper room germicidal UV air disinfection with air mixing was highly effective in reducing tuberculosis transmission under hospital conditions and included improved evidence-based dosing guidelines.

Through the years, UV-C light has been proven to inactivate, without exception, all micro-organisms and viruses against which it has been tested, including, among others, those causing tuberculosis, influenza and SARS-CoV-1 [12].

THE SCIENTIFIC BASICS OF UV-C GERMICIDAL EFFICIENCY ARE WELL UNDERSTOOD

Ultraviolet Germicidal Irradiation is electromagnetic radiation that destroys the ability of pathogens to reproduce by causing photochemical changes in nucleic acids. The wavelengths in the UV-C range are particularly damaging to pathogens because they are absorbed by proteins, RNA, and DNA. The germicidal effectiveness of UV is typically represented by the graph shown in Figure 1 and originally published by Gates in 1930 [13]. The germicidal action spectrum with peak effectiveness at 265 nm coincidentally overlaps with the 253.7nm peak of low-pressure mercury UV lamps. Although the germicidal effectiveness can vary between species, the curve for E. coli is very typical for common pathogens.

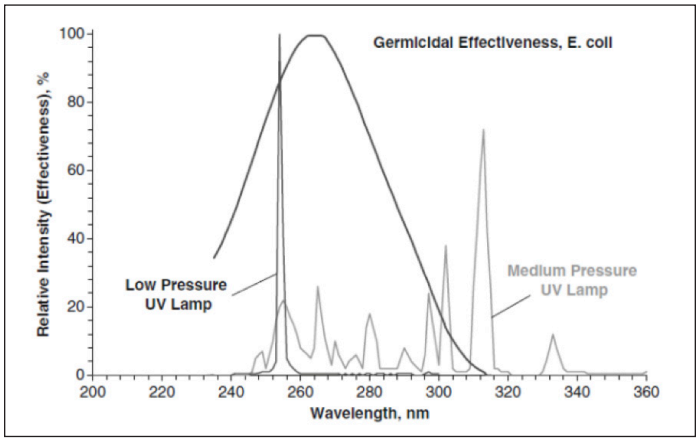

Figure 1. Germicidal efficiency of UV wavelengths, comparing High (or medium) and low-pressure UV lamps with germicidal effectiveness for E. coli. [18]

UPPER-AIR UV-C SYSTEMS CAN INHIBIT THE LIKELY AIRBORNE TRANSMISSION ROUTE OF SARS-COV-2

Several studies indicate that airborne transmission is a significant factor in the spread of the SARS-CoV-2 virus and of other viruses that cause diseases like SARS, MERS, and influenza [14][15] [16]. On 30 April 2021, the WHO updated its Q&A page with a warning of airborne transmission of SARS-CoV-2 to say "The virus can spread from an infected person's mouth or nose in small liquid particles when they cough, sneeze, speak, sing or breathe. These particles range from larger respiratory droplets to smaller aerosols." [17]. Airborne transmission is further backed up by scientific publications describing, for example, the Skagit Valley chorale superspreading event [18], [19], [20], [21].

Natural air flows resulting from movement, temperature changes and recirculating air-conditioning in indoor spaces contribute to the rapid spread of viruses like SARS-CoV-2. This is an obvious challenge in battling the virus, as air cannot be easily contained. However, the risks can be mitigated by applying UV-C light to reduce the virus concentration in the air using in-duct and upper-air disinfection systems, while at the same time preventing human exposure to UV-C irradiation. Indeed, both solutions leverage air flow models to provide the right UV-C intensities to achieve effective disinfection.

Recently, both the WHO and CDC recommended [22][23] the use of upper-room UVGI systems as a supplemental air-cleaning measure to reduce the transmission of airborne pathogens in

public buildings, hospitals, military housings, and classrooms.

THE METRICS BEHIND UV-C EFFECTIVENESS ASSESSMENT

The first theoretical models describing the UV disinfection process and related decay models were described by Hiatt in 1964 [24]. The UV-C effectiveness is typically expressed as the fraction of pathogens killed or inactivated by the UV-C irradiation compared to the situation without UV-C irradiation [25]. How many pathogens are inactivated as a result of UV exposure depends on the received UV dose D and the UV susceptibility k (the 'k-value') of the pathogen. Theoretically, the higher the k-value for a target pathogen, the more quickly the pathogen will be killed or inactivated by UV-C irradiation:

$$N_{UV} / N_0 = e^{-kD}$$

where N_0 is the number of surviving microorganisms with no UVGI exposure,

N_{UV} is the number of surviving microorganisms following UV exposure, and

D is the UVGI dose

As indicated by this formula, pathogens exposed to UV-C irradiation typically decrease exponentially. Another common metric that is used to quantify the effectiveness of UV-C irradiation is the UV-C dose required to inactivate 90% of the initial population: D90. The corresponding D90 values for a wide range of pathogens can be found in UVGI handbooks (e.g., Kowalski [25]) but also in standards like ISO 15714 [26]

Log Reduction Value (LRV) (sometimes called Log reduction factor)

Log reduction is commonly used to express the relative number of pathogens inactivated by disinfection. A 1-log reduction corresponds to inactivating 90 percent of a target pathogen, or equivalently a reduction of the pathogens count by a factor 10. Respectively, a 2-log and 3-log reduction correspond to inactivating 99% and 99,9%, or equivalently a reduction by a factor 100, 1000.

$$\text{Log reduction} = \log10 (N_0 / N_{UV}) \qquad \text{(Equation 1)}$$

UV dose and susceptibility

Effective disinfection systems achieve the desired log reduction factor by using the adequate level of pathogen-specific UV-C dose.

Every pathogen, based on its biological make-up, has a unique spectral susceptibility, which is characterized with the coefficient k in the previous equation. Scientific studies have shown so far that all tested pathogens are inactivated by UV-C, and SARS-CoV-2, the virus that causes COVID-19, is no exception [27]. However, the exact UV-C susceptibility of SARS-CoV-2 has not been measured and reported yet. Nevertheless, data on other (corona)viruses is available.

One of the first quantitative measurements of the effect of UVGI on one of the coronaviruses was performed by Walker and Ko [20] in 2007. They performed experiments on coronavirus aerosols in a single pass test rig. They measured a k-value of 0.377 m^2/J for the Murine (Mouse) Hepatitis Virus (MHV) coronavirus.

An overview of the key experimental UV-C air and surface disinfection at 254nm studies is shown in *Table 1*.

The relatively high k-value measured for the MHV Coronavirus suggests that UV-C disinfection may be an effective tool for inactivating the coronaviruses that cause diseases such as SARS, MERS as well as COVID-19. Beggs et al. [31] made an analysis of this data and other data available in literature to predict a 'most likely range for k-factor of 0.377-0.590 J/m2 for SARS-CoV-2. This overview provides evidence that coronaviruses are as susceptible to UV-C disinfection when aerosolised as M. tuberculo-

Pathogen type	Surface			Air		
	K-value (m^2/J)	D90 dose (J/m^2)	Source	K-value (m^2/J)	D90 dose (J/m^2)	Source
SARS-CoV-2	0.063-0.092	25-36.7	Boston University / Signify [29]	0.377 predicted value (MHV Coronavirus)	6 predicted value (MHV Coronavirus)	Walker [25]
Mycobacterium tuberculosis	0.096	24	Collins [30]	0.472	5	Riley [9]

Table 1. Examples of measured characteristics of pathogens and responses to UV-C

sis. In general, aerosolized viruses appear to be more vulnerable to UV damage than those suspended in a liquid or remaining on surfaces. Therefore, ASHRAE (The American Society of Heating, Refrigerating and Air-Conditioning Engineers) are working on UVGI UR Guidelines [32].

MODELING UPPER AIR DISINFECTION WITH UV-C LUMINAIRE

When designing upper room disinfection systems based on UV-C, the key requirements are ensuring that people in the room are safe and the air is adequately disinfected. The first requirement is strongly dependent on the wavelength chosen for UV-C disinfection and the design of the luminaire itself. The second requirement depends on the dose received by the pathogens, which is determined by the actual air flow in the room in combination with the irradiance distribution in the UV-C disinfection zone. We will now focus on simulation of the latter.

Three elements are included in the simulation: the airflow in the room, the bio-aerosols released by a sick patient, and the irradiance from the UV-C luminaire.

The respiratory particles released by a sick patient normally can be categorized as being in one of three states. Large droplets often only travel short distances before falling to the floor. Depending on the conditions, such as temperature and humidity, smaller particle may either evaporate or remain as aerosols and travel further. These are of the greatest interest because they can stay in the air for longer times and potentially contaminate people. For the sake of simplicity in this present paper, only aerosols which mix with room air are modelled.

A 3D virtual model of a room with mechanical ventilation can be described as follows. It contains the room dimensions, the number of air changes per hour (ACH), determined by the ventilation (HVAC) system, the UV-C disinfection zone, which is dependent on the number of luminaires and their location, the person zone (where people are standing or sitting), the released contaminated aerosol, and the type of contaminant e.g., SARS-CoV-2. A schematic illustration of such a room is shown in *Figure 2*).

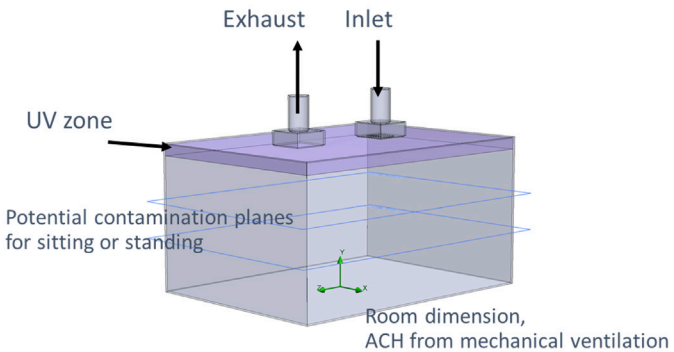

Figure 2. Example of simplified room model with mechanical ceiling ventilation

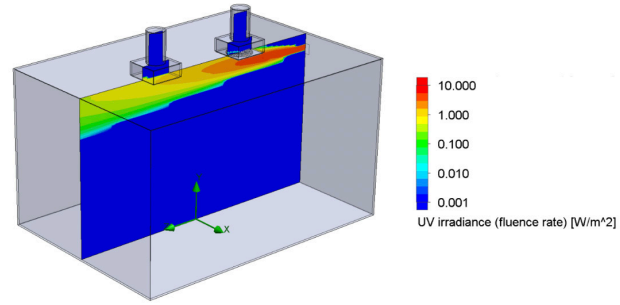

Figure 3. Example of UV irradiance for a UV source located on the back wall near the ceiling

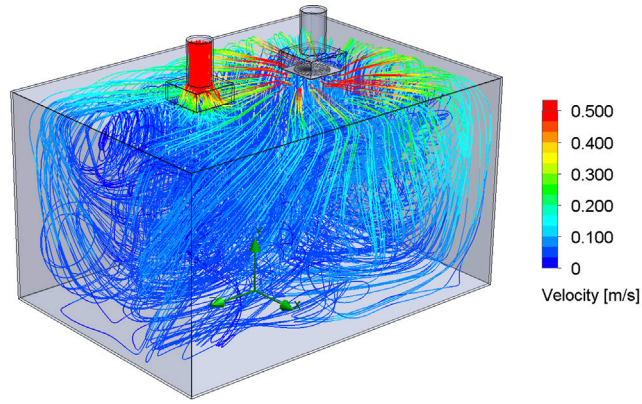

figure 4. Example of airflow simulation + particle trajectory

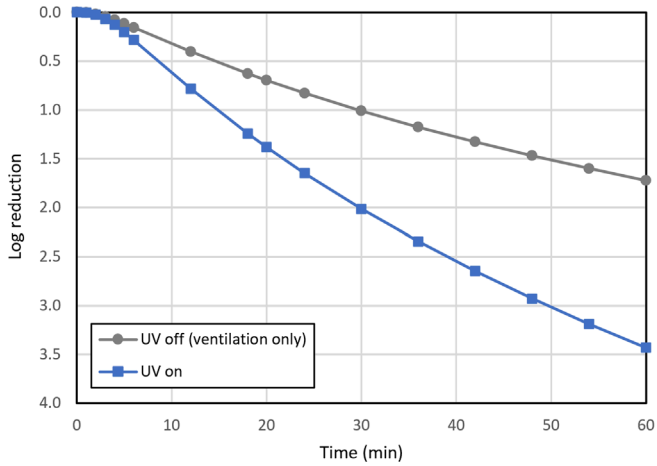

figure 5. Log reduction of virus @ACH

Numerous commercially available simulation tools are available for this type of modeling. This example used a tool that is capable of combining all of the above mentioned critical elements [32].

Figure 3 and *Figure 4* show examples of irradiance and airflow distribution in the modeled room.

In the air flow simulation particles were tracked over time. From the location history of the particles and the UV irradiance in the room, the UV dose accumulated by the particles is determined. Additionally, it is checked whether a particle is still in the room at a given time. This information can then be used to determine the remaining concentration of active pathogens in the room using equation (1). Alternatively, it can be checked how many particles have reached a certain threshold dose, such as D90.

Expressed in log reduction, *Figure 5* shows a typical output for both cases with and without UV-C disinfection. In this particular example, the plot shows for instance that after 30 minutes, using UV dose together with ventilation achieves a 2-log reduction while with solely ventilation, only a 1-log reduction is achieved.

ADVANTAGES OF USING ANALYSIS METHODS SUCH AS COMPUTATIONAL FLUID DYNAMICS

In summary, considering the difficulty and related risks of doing experiments with an active lethal virus, being able to provide 3D simulations of the target applications presents a substantial advantage to quantify and further optimize the efficacy of UV-C disinfection systems. It also provides objective metrics to compare the germicidal efficacy of different engineering air disinfection technologies. Thereby, the air disinfection efficacy can for example be expressed using the log reduction value as a function of time. Optimizing upper room UV C systems using analysis methods, such as computational fluid dynamics, will be essential in the fight against present and future airborne diseases, like SARS-CoV-2.

REFERENCES

1. Johns Hopkins: COVID-19 Map - Johns Hopkins Coronavirus Resource Center (jhu.edu) (Accessed May 14th, 2021)
2. Harvard medical school - Center for global health delivery: https://ghdcenter.hms.harvard.edu/keeping-public-spaces-safe (Accessed May 4th, 2021)
3. Nardell et Al, "Air Disinfection for Airborne Infection Control with a Focus on COVID-19: Why Germicidal UV is Essential", Photochemistry and Photobiology, 2021, 97: 493–497
4. Schmarda LK. Der Einfluss des Lichtes auf die Infusionsthierchen. Med Jahrbücher des k. k. Österreichischen Staates. 1845;54:257–70
5. Downes A, Blunt R.P., "Researches on the Effect of Light upon Bacteria and Other Organisms", Proceedings of the Royal Society of Medicine, 26; 488, 1877
6. Wells WF, Fair MG. "Viability of B. coli exposed to ultra-violet radiation in air.", Science 1935;82:280-1.
7. Riley RL, Wells WF, Mills CC, Nyka W, McLean RL [1957]. Air hygiene in tuberculosis: quantitative studies of infectivity and control in a pilot ward. Am Rev Tuberc 75(3):420-431.
8. Riley RL, Mills CC, Nyka W, Weinstock N, Storey PB, Sultan LU, Riley MC, Wells WF [1959]. Aerial dissemination of pulmonary tuberculosis: a two-year study of contagion in a tuberculosis ward. Am J Hyg 70:185-196
9. Riley RL, Knight M, Middlebrook G. Ultraviolet susceptibility of BCG and virulent tubercle bacilli. Am Rev Respir Dis 1976;113:413-8.
10. Escombe AR, Moore DAJ, Gilman RH, Navincopa M, Ticona E, Mitchell B, et al. Upper-room ultraviolet light and negative air ionization to prevent tuberculosis transmission. PLoS Med 2009;6:e43.
11. M.Mphaphlele, E.A. Nardell, "Controlled Trial of Upper Room Ultraviolet Air Disinfection: A Basis for New Dosing Guidelines", Am J Respir Crit Care Med Vol 192, Iss 4, pp 477–484, Aug 15, 2015
12. A.H. Malayeri, M.Mohseni, B.Cairns, J.R.Bolton, "Fluence (UV Dose) Required to Achieve Incremental Log Inactivation of Bacteria, Protozoa, Viruses and Algae", (2016), www.iuvanews.com/stories/pdf/archives/180301_UVSensitivityReview_full.pdf
13. Gates FL. A study of the bactericidal action of ultra violet light: III. The absorption of ultra violet light by bacteria. J Gen Physiol 1930;14:31-42.
14. E.A.Nardell, R.R. Nathavitharana, "Airborne Spread of SARS-CoV-2 and a Potential Role for Air Disinfection", JAMA. 2020;324(2):141-142
15. [24] L.Marr, S.Miller, K.Prather, C.Haas, W.Bahnfleth, R.Corsi, J.Tang, H.Herrmann, K.Pollitt and J.L.Jimenez, "FAQs on Protecting Yourself from COVID-19 Aerosol Transmission", https://tinyurl.com/FAQ-aerosols (2020)
16. [25] https://www.medrxiv.org/content/10.1101/2020.10.13.20212233v1
17. WHO website: Coronavirus disease (COVID-19): How is it transmitted? (who.int) (accessed May 14th, 2021)
18. Transmission of SARS-CoV-2 by inhalation of respiratory aerosol in the Skagit Valley Chorale superspreading event. doi.org/10.1101/2020.06.15.20132027
19. E.A.Nardell, R.R. Nathavitharana, "Airborne Spread of SARS-CoV-2 and a Potential Role for Air Disinfection", JAMA. 2020;324(2):141-142
20. L.Marr, S.Miller, K.Prather, C.Haas, W.Bahnfleth, R.Corsi, J.Tang, H.Herrmann, K.Pollitt and J.L.Jimenez, "FAQs on Protecting Yourself from COVID-19 Aerosol Transmission", https://tinyurl.com/FAQ-aerosols (2020)
21. https://www.medrxiv.org/content/10.1101/2020.10.13.20212233v1
22. WHO guidelines on tuberculosis infection prevention and control (2019 update)
23. https://www.cdc.gov/infectioncontrol/pdf/guidelines/environmental-guidelines-P.pdf
24. Hiatt C. 1964. "Kinetics of the inactivation of viruses." Bact Rev 28(2):150–163.
25. W.Kowalski, "Ultraviolet Germicidal Irradiation Handbook, UVGI for Air and Surface Disinfection", 2009
26. ISO 15714, "Method of evaluating the UV dose to airborne microorganisms transiting in-duct ultraviolet germicidal irradiation devices", Edition 2019-07
27. Innovative Bioanalysis. Efficacy of a wall mounted UV

device against aerosolized SARS-CoV-2 https://www.assets.signify.com/is/content/Signify/Assets/philips-lighting/global/20210301-innovative-bioanalysis-report-sars-cov-2.pdf. (accessed May, 28th 2021)
28. C.M.Walker, G.Ko, "Effect of Ultraviolet Germicidal Irradiation on Viral Aerosols", Environ. Sci. Technol. 2007, 41, 5460-5465
29. N.Storm, L.McKay, S.Downs, R.Johnson, D.Birra, M.de Samber, W.Willaert, G.Cennini, A.Griffiths, "Rapid and complete inactivation of SARS-CoV-2 by ultraviolet-C irradiation", pre-print version
30. F.M. Collins, "Relative Susceptibility of Acid-Fast and Non-Acid-Fast Bacteria to Ultraviolet Light", applied microbiology, Mar. 1971, p. 411-413
31. Beggs CB, Avital EJ. 2020. Upper-room ultraviolet air disinfection might help to reduce COVID-19 transmission in buildings: a feasibility study. PeerJ 8:e10196 DOI 10.7717/peerj.10196
32. ASHRAE, Ultraviolet air and surface treatment, Handbook Chapter 62, https://www.ashrae.org/file%20library/technical%20resources/covid-19/i-p_a19_ch62_uvairandsurfacetreatment.pdf (Accessed May 2021)
33. FloEFD computer fluid dynamics simulation tool from Siemens. Simcenter FLOEFD | Siemens Digital Industries Software (Accessed May 2021)

Future Trends in LED Driver System Modeling

P. Watté
Signify Research, High Tech Campus, Eindhoven, The Netherlands

Introduction

A decade ago, the major players in the lighting industry decided to make the transition to digital systems and set the pace in connected lighting. At present, only a few companies can maintain their leadership. As a self-fulfilling prophecy, the lighting landscape changed remarkably, with scattered competitors having access to internet of things (IOT) ecosystems (e.g., Amazon Alexa, Google Home, Apple Home kit, …). Solid state lighting systems became commodities: warranty periods and product life outperform what was ever achievable with conventional technology. As such, lighting business models turned more towards service-based contracts.

Good product life prediction capability marks a competitive advantage, both for the lighting manufacturers as well as the end users. It allows improved maintenance schedules and enables greater transparency in defining requirements for the spare part stock. This article describes the background and basis of an in-house electronics reliability tool that has been developed to improve reliability predictions.

In *Figure 1*, a pie chart of the root causes of the failures of lighting systems is depicted. It originates from a generic study in the LED lighting world [1]. This chart, with data from up to 2014, shows that electronic failures can be responsible for up to 40% of the total field returns of LED systems. This illustrates the critical need for user-friendly tools to estimate the field returns of LED drivers. More refined modelling capabilities will help to further bring down this contribution.

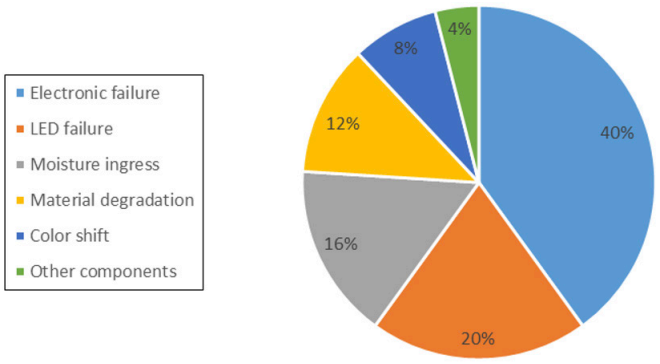

Figure 1. pie chart of the most common electronics failures in LED systems [1]

Trends and Challenges in LED Driver Life Modeling.

There are some market trends, many of them the result of technology push, that shed a new light on the current quality and reliability approaches in the lighting industry.

First, there is a tendency towards miniaturization. In order to enhance the design-in degrees of freedom of drivers, the LED driver size becomes a unique selling point. Although from an architectural point of view, LED drivers do not feature extreme high complexity, they must deal with a myriad of field mission profiles as well as potential issues in public electricity grids that can lead to voltage dips and surges. Temperature constraints need to be addressed up-front in the development process, preferably using prototyping tools, which will be shown hereafter.

With the advent of connected lighting, the use of sensors and wireless technology became widespread. As such, LED drivers include more features, such as passive infrared sensors (PIR) and microwave sensors, that may be used for presence detection. In outdoor applications, light poles communicate with servers that store information (electrical signals, temperature, application mission profiles, etc.). The resulting data sets are highly suited for prognostics purposes.

To guarantee flawless operation during the projected service life, LED drivers are predominantly tested in well-equipped labs with state-of-the-art test facilities. Development teams follow detailed test validation plans to reduce product risks over the project execution. The most commonly executed tests are thermal cycle and shock tests, relative humidity tests, salt mist tests, surge tests, damp heat tests, vibration and mechanical shock tests. The challenge is to integrate knowledge from previous tests into a dedicated modelling tool. In a circular economy, where customer service prevails, the power to predict remaining system life becomes an important asset. Therefore, data analysts and reliability engineers are joining forces to bring prognostics to a higher level. This cannot be done without validation from physics of failure models.

Speaking the Language of rReliability: Modelling the Bath-tub Curve

The bathtub curve is a practical vehicle to illustrate the quality and reliability along the life cycle of LED drivers. Infant mortalities are not accounted for in the presented model. That is because

MEOST (multiple environment overstress tests) [2] and the application of FMEA's or burn-in are successfully used to avoid this first stage of decreasing failure rate.

The well-known parts count method in reliability [3,6] is employed to construct the flat part, using the base FITs (failure in time, in which the time is a billion hours of operation) of the components of the board assembly. For calculation purposes, the latter are corrected for local temperatures, using Arrhenius approaches. For electrolytic capacitors (ELCAPs), ripple currents and local temperatures are accounted for since the latter determine the failure rate.

The third part of the bathtub curve pertains to the wear out. We know from history that solder joint cracking and degradation of electrolytic capacitors are the most important wear out failures for LED drivers. Dedicated physical and empirical models are (being) built and maintained to be integrated in our prototyping tools.

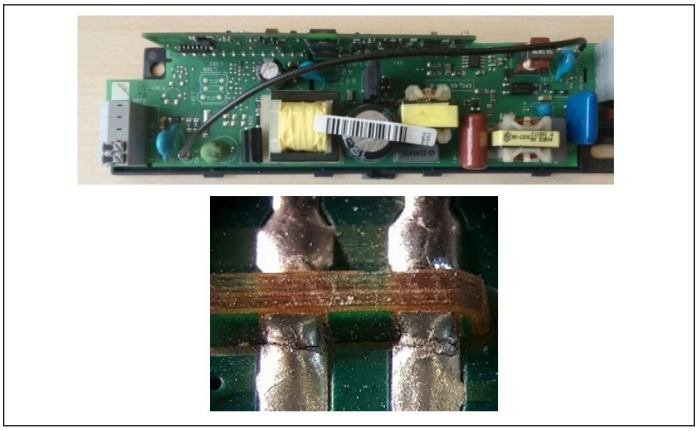

Figure 2. board to board solder joint connects for mother-daughter board PBA configurations (top), cracked board-to-board connections (bottom)

Unless proven otherwise, a LED driver is generally perceived as the weakest link in the system. For random failures, the modelling is rather straightforward, and the parts count method is applied. Various FIT and design analysis calculators are commercially available [3-5]. However, it is often unclear to users which approach to select amongst the possible standards, ... some being more conservative than others. Some companies derive product warranties only from their own data. In the example hereafter, a repository of historical data inherited from validation tests originating from Philips/Signify is used. The correction formulae for temperature and deratings are like the ones advocated in the IEC 61709 guideline [6].

For wear out, the focus is chiefly on ELCAP degradation and solder joint fatigue, because these failures are dominant in validation tests under stressed conditions (and are also reported as field returns). Because of practical considerations, the scope is confined to the most critical solder joints. From experience, it is known that two types of solder joints are the most vulnerable to fatigue cracking [7-8].

- Through-hole components like large transformers, can be quite susceptible to solder fatigue cracking, especially when they have large dimensions, combined with relatively large thermal expansion coefficient (CTE) mismatches with the printed boards.
- Board-to-board connections are also critical, in cases when there is a strong mismatch in CTE and the insertion length of the daughter in the mother board is relatively large, as illustrated in *Figure 2*. Stresses are imposed not only during the application of thermal/power cycles, but also during the thermal excursions used in wave solder. The latter stresses are generally retained as residual stresses within the assembly when it cools down to room temperature. This especially occurs when dealing with lead-free solders, due to the higher reflow temperatures.

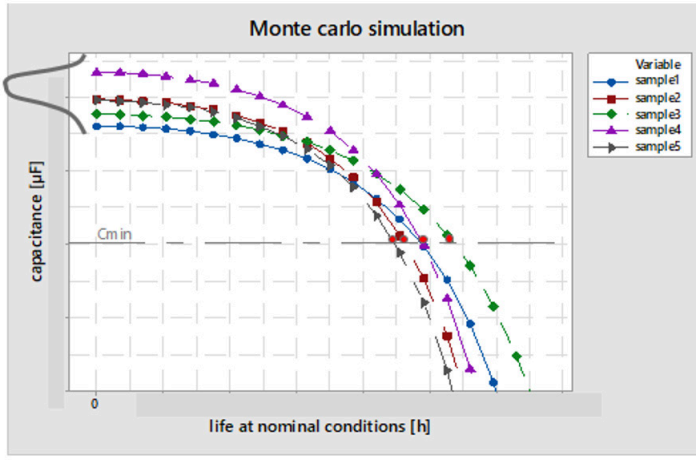

Figure 3. typical shape of the degradation curves of electrolytic capacitors (ELCAPs), due to operational temperature. Cmin is the minimum threshold capacitance, imposed by the application

A second potential source for wear out failures is the electrolytic capacitors [13-14]. Aluminum electrolytic capacitors are fabricated by interleaving paper between two strips of aluminum foil. Foil and paper are wound into an element and impregnated with electrolyte. Such ELCAPs can degrade over time due to ageing of the dielectric, foil degradation, oxide film degradation, and the dry out of the electrolyte [13-14].

Degradation of electrolytic capacitors is modeled in our analysis by means of a stochastic method. Variance is assumed on the initial capacitance value and on the shape of the degradation curve. *Figure 3* displays a set of degradation curves that results from Monte Carlo simulations. Companies partnering with ELCAP suppliers have access to their validation tests and hence know the typical shapes of the degradation curves. In the example in *Figure 3*, the shapes are approximated as the envelope of multiple linear decreasing parts or stages.

When all former elements are available, it is possible to construct the overall reliability curve as the convolution of the following reliability functions [9-12]:

In *Equation 1*, 'W.O." denotes the wear out and "rand" points to random failures. L is the number of components populated on the printed board, M the number of electrolytic capacitors and N the number of critical solder joints. Rather than working with the bath-tub curve, the tool depicts the cumulative probability curve for failure as a function of time, F(t)=1-R(t). Failure points are determined on this function F(t) via Newton Raphson root finding.

$$R_{system}(t) = \prod_{i=1}^{L} R_i^{rand,comp}(t) \times \prod_{j=1}^{M} R_j^{elcap,W.O.}(t) \times \prod_{k=1}^{N} R_j^{solder,W.O.}(t) \qquad \text{Eq 1}$$

For the solder reliability functions in the third part of *Eq 1*, designed experiments (DoE), in which the laminate choice of the mother board (or CTE mismatch with the daughter card) was varied, were conducted. Other factors in the DoE were the daughter card length and the solder paste. Fatigue experiments were set up with 2 settings of the thermal cycle temperature range (ΔT), with well-defined dwell times and ramp times. From this testing, empirical design rules were generated for the cumulative failure probability and are used in the computation for broad level solder joint reliability, shown in *Eq 2*.

$$R_{\text{solder joint}}(t, \Delta T) = exp\left(-\left[\frac{t}{\alpha(\Delta T)}\right]^{\beta}\right) \qquad \text{Eq. 2}$$

With α(ΔT) a design rule for the 63% failure point as a function of the DoE parameters, determined via a maximum likelihood (MLE) fit of the failure data.

Integration into a Calculator.

The various building blocks described in paragraphs 2-3 were integrated into a calculator developed for use by validation and quality engineers as well as system architects.

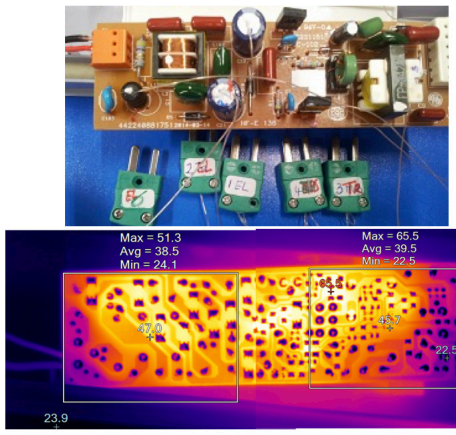

figure 4. on bread boards (top) or released printed board assemblies (bottom), local hot spots are determined. This info serves for the calculation of the system mean time to failure (MTTF) and the Bx failure points

The input to the calculator listed in *Table 1* mainly consists of printed board information, solder materials, ELCAP families, design and use-conditions. In the current example, a typical outdoor mission profile is chosen. The design characteristics are traded-off versus the application conditions. In case the design is over-specified, FIT de-ratings are applied using correction factors as proposed in [6], or vice versa. Component dimensions are needed to calculate solder joint life by accounting for shear deformation and creep relaxation. The printed board laminate must be specified to determine mismatches in thermal expansion with the components. Temperature inputs are based on measurements at breadboards for typical use conditions (i.e. the mission profiles encountered in the field). To this purpose, infrared or thermocouple measurements are conducted to identify hot spots, as illustrated in *Figure 4*. Alternatively, it can be based on T_{case} temperatures measured at final driver topologies at full operation, in the dimmed state and after self-heating in the luminaire. By means of the Miner's rule for accumulated loadings [11-12], this temperature information is used to compute the equivalent failures in time.

A bill of material file, which contains the so-called TVI (Temperature, Voltage derating and I_{ripple}) information, serves as additional input. For each component, information is gathered about the local temperature, the power and voltage derating and for the ELCAPs ripple current deratings.

An example of a calculation is given in *Figure 5*. The green curve labels the cumulative failure probability of the driver system. The black curve does the same for the ELCAP in the driver's bill of material. The blue and the red curve refer to the failure probability of the solder interconnects and the components respectively. *Figure 5* shows that for the computed example wear out of the electrolytic capacitor is more critical than the solder joints, what is reflected in the shape of the system failure curve. The left tail is important for the determination of the 5 and 10 percent failure points of the driver.

printed board inputs		product strength specs	
Laminate	FR4	surge protection	tested
Solder	SAC305	humidity design	protection
L_daughter card [mm]	150	mechanical design	pass 5G
Diam betw 2 pins conductor [mm]	12	application use conditions	
Cap dimensions x E [E = 2.5 mm]	1	surges and dips	clean mains
application use conditions	outdoor	humidity use	can occur
		mechanical use	outdoor
		lightning protection use	10 kV

Table 1. input example for the ERT calculation

The graphical output in *Figure 5* allows information from a prototyping phase to be used to estimate the projected lifetime of a LED driver. A table with the corrected FIT numbers for each component can also be retrieved. In case of outliers in those numbers, it is easy to pinpoint the suspected components for doing design iterations. Once the design has been finalized, the tool can be used to establish product warranties. This framework is indispensable when aiming to build digital twins to assess the rest life of products in the field. In the future, this calculation tool will be made adaptable for such analyses.

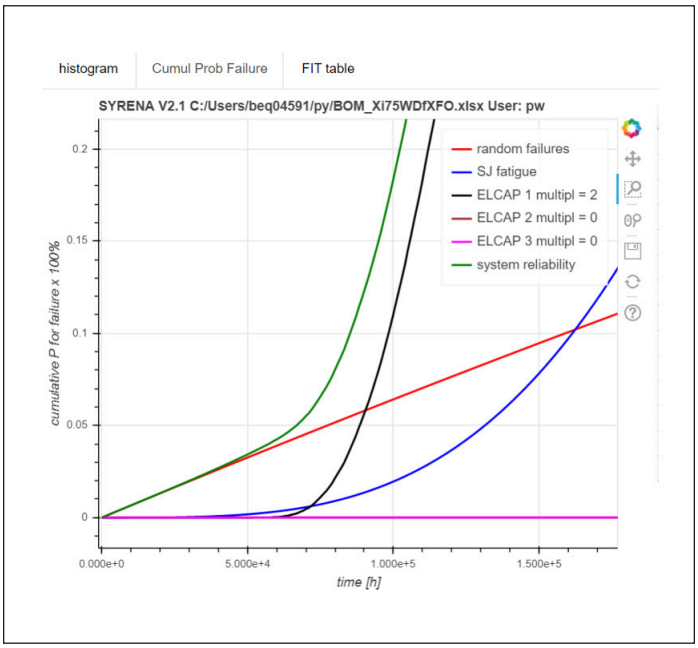

Figure 5. cumulative probability for failure as a function of lifetime for an uploaded bill of material

Conclusions and Outlook

Reliability is an important driver to win in LED service contracts. As product maturity increases, customers and original equipment manufacturers (OEM's) are entitled to ask the rationale behind the derivation of specifications. Leading companies with a design for reliability mindset can easily provide such requested transparency.

It remains worthwhile devoting resources to experimental validation testing and modeling of new LED and driver platforms. These can provide the basis for calculators backed up by powerful physics of failure (PoF) models and a FIT repository.

Product life prediction using log data from built-in sensors or canary devices becomes the new reliability paradigm. This information will be used to train deep learning models, hybrid reliability models and digital twins. The use of big data analytics on the available data sets has the potential pitfall to become an unguided projectile, if not supported by any PoF model. Accordingly, work remains to be done to crystallize all the good initiatives. Having a permanent focus that continuously refines reliability models and updates correction formulae is key to successfully improve reliability prediction.

References

[1] Next Generation Lighting Industry Alliance LED Systems Reliability Consortium, LED luminaire lifetime: recommendations for testing and reporting, 3rd edition, 2014.
[2] K. Bhote and A. Bhote, "World Class Reliability using multiple environment overstress testing (MEOST) to make it happen", AMACOM, (2004)
[3] FIDES guide 2009 Edition A, September 2010 Reliability Methodology for Electronic Systems
[4] https://www.dfrsolutions.com/what-is-sherlock-ansys
[5] https://www.ptc.com/en/products/plm/plm-products/windchill
[6] IEC 61709, "Electric components – Reliability – Reference conditions for failure rates and stress models for conversion", Ed 3.0, (2017)
[7] J.P. Clech, "ACCELERATION FACTORS AND THERMAL CYCLING TEST EFFICIENCY FOR LEAD-FREE SN-AG-CU ASSEMBLIES", presented at SMTAI Chicago, IL, (2005)
[8] W. Engelmaier, "Solder Joint Reliability - Theory and Applications", ed. J.H. Lau, Van Nostrand Reinhold, New York, (1991), 545
[9] M. Rausand and A. Hoyland, "System Reliability theory", Wiley, (2003)
[10] W. Van Driel and X.J. Fan, "Solid state lighting reliability: components to systems", Springer, (2013)
[11] P. O'Connor, "Practical Reliability Engineering",Wiley (2002)
[12] D. Crowe and A. Feinberg, "Design for reliability", CRC Press, (2001)
[13] S. Gulbranson, "Accelerated aluminum electrolytic capacitor life testing", DfR Solutions, not published
[14] T. Ashburn, D. Skamser, SMTA Medical Electronics Symposium – Anaheim, California – 2008

Acknowledgments

Prof. W.D. Van Driel, X.J. Zhao, H. De Vries, G. Van Hees, U. Boeke and R. Engelen are gratefully acknowledged for the stimulating discussions and the sharing of data for this article.

thermalLIVE

OCTOBER 19-20 2021

ONLINE EVENT

The Largest Single Thermal Management Event of The Year - Anywhere.

Thermal Live™ is a new concept in education and networking in thermal management - a FREE 2-day online event for electronics and mechanical engineers to learn the latest in thermal management techniques and topics. Produced by *Electronics Cooling*® magazine, and launched in October 2015 for the first time, Thermal Live™ features webinars, roundtables, whitepapers, and videos... and there is no cost to attend.

For more information about Technical Programs,
Thermal Management Resources, Sponsors & Presenters

please visit:

www.thermal.live

presented by | electronics COOLING

Comparing Populations

Ross Wilcoxon
Associate Technical Editor for *Electronics Cooling*
Collins Aerospace

INTRODUCTION

Previous articles in this series described the normal distribution and how it is used to relate probability and confidence levels [1, 2]. A practical application of the use of the confidence interval was to describe how to determine the range of values in which the true mean of a population falls within, based on the mean and standard deviation calculated from a set of samples drawn from the population. This range depends on the confidence level that is selected for the analysis and the number of samples used to estimate the population. The fewer samples or the higher the confidence level that is selected, the wider the range in which the true mean value may lie.

This article discusses how the confidence band concept is extended to compare different sample sets to determine, within a set confidence level, whether the two sample sets have the same mean. This provides a statistically established method to determine if two data sets are different, thereby demonstrating whether a treatment, design change, etc., lead to an improvement.

The following example illustrates the overall procedure for comparing two populations to determine whether they are different. Somewhat rudimentary testing[1] was used to evaluate a natural convection heat sink in the three different orientations illustrated in *Figure 1*. In the Horizontal orientation, the base of the heat sink was aligned with the direction of gravity and the fins were perpendicular to gravity. In the Vertical orientation, the heat sink base was again aligned with gravity, but the heat sink was rotated 90° such that the fins were parallel to gravity. In the Flat orientation, the fins faced upwards with the base perpendicular to the direction of gravity. *Table 1* shows individual thermal resistances calculated from different tests and calculated values for the number of data points (n), mean (μ), and standard deviation (σ) for each heat sink orientation. In this testing, power was dissipated from a heater attached to the back of the heat sink. The average heat sink temperature was determined with four thermocouples attached to the heat sink and the thermal resistances were calculated by dividing the temperature difference (average heat sink temperature minus ambient air temperature) by the heater power dissipation. Tests were repeated over a number of days with different heater powers and with the orientations relative to gravity randomized. Testing did not control for the effects of radiation, minor room drafts, heat losses from the back of the heat sink, etc. Therefore, the data shown in *Table 1* are primarily useful for comparing the effects of orientation, and do not represent a controlled investigation to determine the precise heat sink resistances. While testing was conducted over a broad range of power dissipations, the data in *Table 1* are limited to rest data for power dissipation in the range of 20-25W.

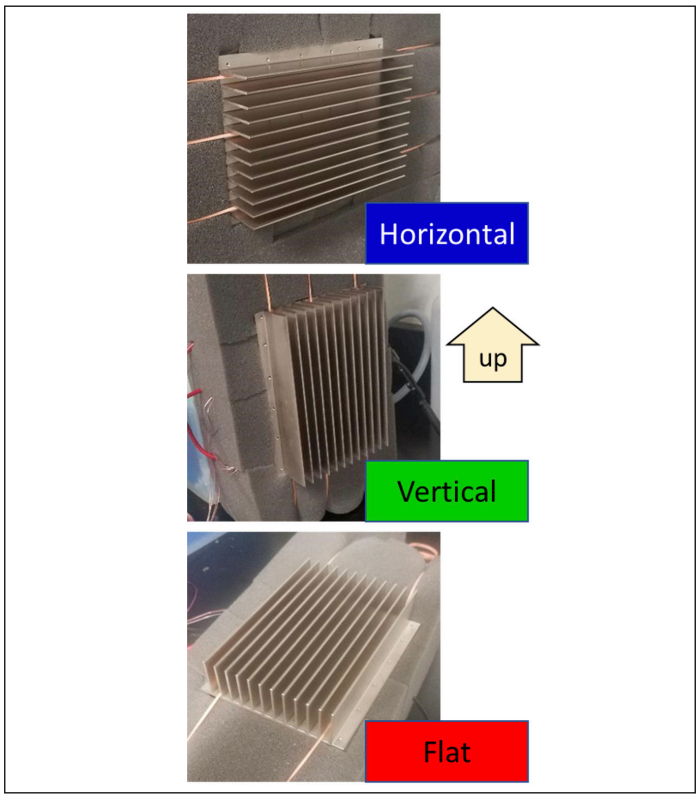

Figure 1. Heat sink orientations for natural convection testing

[1] Note the rubber bands and packing foam used in the test setup

	Horizontal	Vertical	Flat
Calculated Thermal Resistance Values (K/W)	3.75	1.82	1.93
	3.80	1.83	1.96
	3.82	1.85	1.97
	3.82	1.85	2.00
	3.94	1.90	2.01
		1.91	2.01
		1.92	2.05
		2.13*	2.08
			2.08
Sample Size	5	8	9
Mean, μ	3.82	1.90	2.01
Std. Deviation, σ	0.0676	0.1003	0.0541

Table 1. Heat sink thermal resistance test data

Based on the sample mean values of the thermal resistances, it appears that the Horizontal orientation has a significantly higher thermal resistance (of 3.82 K/W) than the Vertical orientation (resistance of 1.88 K/W) and the Flat orientation (2.01 K/W). The questions that we will attempt to answer in this analysis are 1) what is our confidence that the Horizontal thermal resistance is actually different from the other orientations and 2) is there a statistically significant difference in the thermal resistances of the Vertical and Flat heat sink orientations?

Using the procedure described in [2], we can use the calculated mean, standard deviation and sample size to determine the range in which the true mean lies, for a given confidence level, of each set of measurements. With fewer than 30 measurements, we assume that they follow a student t-distribution, which is defined as a function of the confidence level and number of degrees of freedom (d.f.), which is equal to n-1 for a single set of measurements. Values of the t-distribution can be found in tables in any statistics text, many online resources such as [3], or software such as Excel. Again, as shown in [2], the range in which the true mean (μ_{true}) of a population is lies is calculated as a function of the measured mean ($\mu_{measured}$),

$$\mu_{true} = \mu_{measured} \pm \Delta, \quad where\ \Delta = \frac{t(c.l.,d.f.)*\sigma}{\sqrt{n}} \qquad \{1\}$$

For example, with the horizontal data, in which 5 measurements produced an average of 3.82 and standard deviation of 0.676, we can be 95% confident that the true mean falls between 3.74 and 3.91 [2]. The parameters used to calculate the confidence intervals and the ranges for the 95% confidence interval for the mean thermal resistance for each of the three heat sink orientations are shown in *Table 2*. This table includes each value of t corresponding to the degrees of freedom (sample size – 1) and the confidence level of 0.025, which is calculated by (1 – 0.95)/2 with the 2 corresponding to a two-tailed distribution.

		Horizontal	Vertical	Flat
Distribution statistics	# samples, n	5	8	9
	Sample mean, $\bar{x}$	3.824	1.901	2.010
	st dev, σ	0.06763	0.1003	0.05414
Parameters for 95% confidence	$t_{0.025}$	2.776	2.365	2.306
	delta, Δ	0.0840	0.0839	0.0416
Range in which mean μ falls	min	3.74	1.82	1.97
	max	3.91	1.98	2.05

Table 2. Terms used to determine 95% confidence intervals for thermal resistance of each orientation

The results in *Table 2* indicate that we can be more than 95% confident that the thermal resistance of the heat sink in the Horizontal orientation is higher than in the other two orientations, since there is no overlap between its range and the others (3.74 is greater than both 1.98 and 2.05). However this approach using a 95% confidence level, indicates the Vertical and Flat thermal resistances are not statistically different since there is a slight overlap in their ranges (1.97 falls between 1.82 and 1.98).

This analysis can be improved by recognizing that the size of the range for a given confidence level is due to a combination of the standard deviations and the number of samples of each test set. Even if the means of two populations are different, their standard deviations may be similar enough that we can 'pool' the data and increase the effective sample size by accounting for the number of samples in each data set.

We can use the F-distribution to determine whether we can pool data to increase the effective sample size. Without going into the detail that it deserves, the F-distribution is a statistical distribution that can tell us the probability that the variances, i.e., standard deviations, of two populations are different – in a similar manner that the t-distribution indicates the probability that the means of two populations are different. We can use the Excel function @f.test(array1, array2) to determine whether the standard deviations of two populations are different, and therefore that data can be pooled to determine the confidence range for the mean. The arrays in that function are the two sets of measurements under

[2]Calculation method: n = 5, μ = 3.824, σ = 0.06763, d.f. = n-1 = 4. 95% confidence for two tailed distribution
=> α/2 = (1-0/95)/2 = 0.025; t-statistic in Excel is $t_{0.025}$ = abs(t.inv(α/2, d.f.) = abs(t.inv(0.025, 4) = 2.7764
Δ = $t_{0.025}$*σ/$n^{1/2}$ = 2.7764*0.06763/$5^{1/2}$ = 0.084, mean range = μ ± Δ = 3.824 - 0.084 to 3.824 + 0.084 = 3.74 to 3.91

consideration and the function returns the probability that the standard deviations are different.

In comparing the Vertical and Flat data, the F-test function returns a value of 10.5%. Since this is greater than 5%, we cannot conclude (at a 95% confidence level) that the variances (standard deviations) of the two populations are different. Therefore, we can pool the data in applying the t-test that determines whether the means of the two population are different. The pooled standard deviation, σ_p, can be calculated using the estimated standard deviations (σ) and sample sizes (n) of each sample set, as shown in *Equation 2* [3].

$$\sigma_p^2 = \frac{(n_1-1)\sigma_1^2+(n_2-1)\sigma_2^2}{n_1+n_2-2} \qquad \{2\}$$

The pooled standard deviation of the Vertical and Flat data is calculated to be 0.006262. This is then used to calculate the test statistic, T, for the pooled data, which is determined with *Equation 3*:

$$T = \frac{|\mu_1-\mu_2|}{\sqrt{\sigma_p^2(1/n_1+1/n_2)}} \qquad \{3\}$$

For the pooled Vertical and Flat data, this is calculated to be 2.8259. This value is then compared to the t-value that is calculated for the selected confidence level and the total degrees of freedom, which is the sum of the samples from the two data sets minus 2 (since one degree of freedom was 'consumed' in calculating each of the two means). For a 95% confidence level and a two tailed distribution, the input parameter for the t-test is $\alpha/2 = (1\text{-}0.95)/2 = 0.025$. In Excel, a value of $\alpha/2$ that is less the 0.5 will return a negative number, so the t-value for the pooled sample can be calculated with =-t.inv(0.025,(8+9-2)) = 2.13144 [3]. Since this value is less than the test statistic of 2.8259, we can be 95% confident that average thermal resistance for the Vertical heat sink is different from the Flat heat sink. If we repeat the analysis with a confidence level of 98.72%, the t-statistic is equal to the T-value of 2.8259. If one prefers to type in fewer equations, a simpler approach to reach the same conclusion is to use the function =1 – t.test(array1, array2, 2, 2), where the two arrays are the two sets of data for the Vertical and Flat orientations. In this function, the first 2 indicates that the distribution is two-tailed, and the second 2 indicates that the two data sets are homoscedastic (with the same variance, as determined by the F-test). This function, with the two sets of data returns a value of 0.9872; since this value is larger than 95%, we can conclude with a 95% confidence level that the thermal resistances for the Flat and Vertical orientations are different.

If the F-test finds that the variance of the data sets ae unequal, the Smith-Satterthwaite procedure [3] can be used to estimate an effective number of degrees of freedom in the pooled data (n_{pooled}) using *Equation 4*:

$$n_{pooled} = rounddown\left\langle \frac{\left[\sigma_1^2/n_1+\sigma_2^2/n_2\right]^2}{\frac{\left[\sigma_1^2/n_1\right]^2}{n_1-1}+\frac{\left[\sigma_2^2/n_2\right]^2}{n_2-1}} \right\rangle \qquad \{4\}$$

where the function rounddown<> rounds the result down to the integer value.

Summary

The t-test provides a method for estimating a range that we can be confident that a population mean falls within, based on a limited sample size. This article described how that can be extended to compare two data sets to determine whether the populations have different mean values. The F-test provides a similar method for determining whether the variances of two populations are the same in order to justify whether two data set can be pooled together to increase the effective sample size and thereby increase the confidence of conclusions.

Author Notes

1. Readers with a reasonable background in statistics may have noticed that I am often a bit careless in my treatment of the mean and standard deviation of a population/sample. A rigorous approach would differentiate between quantities relevant for the complete population (the true mean and standard deviation) compared to the estimated values based on the subset of the population that is sampled. The goal of these article is to provide reasonably simple tools for drawing statistical conclusions without diving too far into the statistical details. I hope that my attempts to minimize confusion that can be generated by additional notations and parameters do not actually increase confusion due to a lack of sufficient context.

2. I slightly modified the data set in order to better demonstrate the impact of pooling data sets. The highest thermal resistance value for the Vertical orientation (2.13, which is indicated with an asterisk) was actually measured to be 1.93 in testing. It is left to the interested reader to calculate how the use of the correct value affects the overall confidence level.

REFERENCES

1. Ross Wilcoxon, "Statistics Corner – Normal Distribution", *Electronics Cooling* Magazine, Summer 2020, pp. 10-11
2. Ross Wilcoxon, "Statistics Corner – Confidence Intervals", *Electronics Cooling* Magazine, Spring 2021, pp. 10-12
3. https://www.tdistributiontable.com/ (accessed May 20, 2021)
4. J. S. Milton and Jesse Arnold, Introduction to Probability and Statistics: Principles and Applications for Engineering and the Computing Sciences, McGraw-Hill, 1986, pp. 297-308

[3]Alternatively, Excel will also return the correct positive value if we use 1-$\alpha/2$: =t.inv(0.975,15) = 2.13144.


Call for Authors
and Contributors!
Want to be a part of the next issue of Electronics Cooling? Have an article or blog post you'd like to write for Electronics-Cooling.com?
Let us know at
editor@electronics-cooling.com
electronics COOLING
www.Electronics-Cooling.com

2021 Company Products & Services Directory

In this section, we provide a quick guide to some of the top suppliers in each EMC category—in heat sinks, thermal testing, design services, and more. To find a product that meets your needs for applications, frequencies, standards requirements, etc., please search these individual supplier websites for the latest information and availability. If you have trouble finding a particular product or solution, email info@lectrixgroup.com for further supplier contacts.

	COMPANY	CONTACT INFORMATION	PRODUCTS & SERVICES
MEDIA PROVIDER SPOTLIGHT	LECTRIX	LECTRIX 1000 Germantown Pike Plymouth Meeting, PA 19462 t: (484) 688-0300 w: www.lectrixgroup.com	– Strategy Firm – Full-Service Marketing – Publishing – Events and Webinars – Custom Solutions – Training and Consultation
	electronics COOLING	Electronics Cooling 1000 Germantown Pike Plymouth Meeting, PA 19462 t: (484) 688-0300 w: www.electronics-cooling.com	– Media – Training Seminars & Workshops
	thermal LIVE 2021	Thermal Live™ 2021 Online Event | October 19th – 20st 2021 t: (484) 688-0300 e: info@electronics-cooling.com w: www.thermal.live	– Training Seminars & Workshops

	COMPANY	WEBSITE	PRODUCTS & SERVICES
A	ALPHA	www.alphanovatech.com	– Coolers – Heat Sinks – Thermal Design Services – Thermal Tapes – Thermal Testing
B	BOYD CORPORATION	www.boydcorp.com	– Blowers/Fan Accessories – Blowers – Chillers – Cold Plates – Fans – Gap Pads & Fillers – Heat Pipes – Heat Sinks – Interface Materials – Liquid Cooling – Thermal Design Services – Thermal Testing
C	Cadence	www.cadence.com/en_US/home.html	– Software
	CEJN USA	www.cejn.us	– Couplings

	COMPANY	WEBSITE	PRODUCTS & SERVICES	
C	Celsia Inc.	www.celsiainc.com	- Heat Pipes - Heat Sinks - Heat Spreaders	- Thermal Design Services - Vapor Chambers
	Concept Group LLC	www.conceptgroupllc.com	- high-performance vacuum insulation	
	CPC	www.cpcworldwide.com	- Connectors	
	COFAN U.S.A.	www.cofan-usa.com	- Blowers - Coolers - Fans	- Heat Sinks - Heat Pipes - TIM's
D	DELTA	www.delta-fan.com	- Blowers - Fan Trays	- Fans - Heat Exchangers
E	ELLSWORTH ADHESIVES	www.ellsworth.com	- Adhesives	- Encapsulants
F	Fujipoly® America Corp.	www.fujipoly.com	- Connectors - Gap Pads & Fillers	- Interface Materials - Thermal Design Services
H	Henkel	www.henkel.com	- Gap Pads & Fillers - Interface Materials - Phase Change Materials	- Substrates - Thermal Tapes
I	Indium	www.indium.com	- Thermal Management Materials	- Thermal Interface Materials
	Institution of MECHANICAL ENGINEERS	www.imeche.org	- Training Seminars & Workshops	
	ims	www.ims-resistors.com	- Heat Spreaders	- Thermal Management Devices
L	Laird Thermal Systems	www.lairdthermal.com	- Thermoelectric Coolers	- Liquid Cooling Systems
M	MALICO INC	www.malico.com	- Cold Plates - Heat Sinks	- Liquid Cooling

	COMPANY	WEBSITE	PRODUCTS & SERVICES	
	MASTERBOND ADHESIVES | SEALANTS | COATINGS	www.masterbond.com	- Interface Materials	
	Mersen	www.mersen.us	- Heat Pipes - Heat Sinks	- Liquid Cold Plates
	MSC Software Corporation	www.mscsoftware.com	- Software	- Training
N	Nanoramic Laboratories	www.nanoramic.com	- Interface Materials	
P	Polymer Science Inc.	www.polymerscience.com	- Gap Fillers - Heat Spreaders	- Interface Materials - Phase Change Materials
R	Rosenberg USA, Inc.	www.rosenbergusa.com	- Blowers - Fan Filters	- Fans
S	Sager Electronics	www.sager.com	- Distributor of Electronics Components	
	SCHLEGEL electronic materials a member of MEI Group	www.schlegelemi.com	- Thermal Interface Materials	- Gap Fillers
	SEMI-THERM	www.semi-therm.org	- Training Seminars & Workshops	
	Shiu Li Technology Co., LTD	www.shiuli.com.tw	- Interface Materials	- Thermal Tapes
	SIEMENS	www.plm.automation.siemens.com/global/en	- Software - Thermal Design Services	- Thermal Testing
	Staubli Corporation	www.staubli.com	- Connectors - Couplings	- Software

	COMPANY	WEBSITE	PRODUCTS & SERVICES
T	T-global Technology Co. Ltd	www.tglobal.com.tw	– Gap Pads & Fillers – Interface Materials – Thermal Tapes
	Thermal Engineering Associates Inc.	www.thermengr.net	– Thermal Test Chips
	TTI, Inc.	www.ttiinc.com	- Distributor of Electronics Components
U	Universal Sciences	www.universal-science.com	- Heatsinks - Peltier devices - Interface materials - Thermal substrates

EMCLIVE

FREE ONLINE EVENT SERIES

EMC LIVE 2021 is a series of **FREE**, online learning events designed for and by engineers in the EMC design and testing space. It features five separate one-day events, each focused on one of the most popular EMC areas in the industry:

Mil/Aero EMC | EMC Testing | Automotive EMC
Wireless/5G/IoT EMC | EMC Fundamentals

Attend an EMC LIVE event to learn the latest in EMC standards, equipment, theory, and design straight from the industry thought leaders.

Available Now

- **MILITARY/AEROSPACE EMC** | WATCH IT HERE ► https://emc.live/2021-event/mil-aero/
- **EMC TESTING** | WATCH IT HERE ► https://emc.live/2021-event/testing/
- **AUTOMOTIVE EMC** | WATCH IT HERE ► https://emc.live/2021-event/automotive/

Coming Soon

- **WIRELESS,5G & IOT EMC** | SEPTEMBER 21, 2021
- **EMC FUNDAMENTALS** | NOVEMBER 9, 2021

All for **FREE** | **WWW.EMC.LIVE**

PRESENTED BY INTERFERENCE TECHNOLOGY

Index of ADVERTISERS

Alpha Novatech, Inc.
473 Sapena Ct. #12,
Santa Clara, CA 95054

t: +1 (408) 567-8082
e: sales@alphanovatech.com
w: www.alphanovatech.com
page: C2

Ellsworth Adhesives
W129 N10825 Washington Drive
Germantown, WI 53022

t: (877) 454-9224
e: info@ellsworth.com
w: www.ellsworth.com
page: 8

EMC LIVE
1000 Germantown Pike
Plymouth Meeting, PA 19462
t: (484) 688-0300
w: https://emc.live/
e: james@lectrixgroup.com
pages: 43

IMS
50 Schoolhouse Lane
Portsmouth, RI 02871

t: (401) 683-9700
e: customerservice@ims-resistors.com
w: www.ims-resistors.com
page: 29

LECTRIX
1000 Germantown Pike,
Plymouth Meeting, PA 19462

t: (484) 688-0300
e: info@lectrixgroup.com
w: www.lectrixgroup.com
page: C4

Malico Inc.
No. 5 , Ming Lung Road
Yang Mei
Tao Yuan 32663

t: (886) 3-4728155
e: inquiry@malico.com
w: www.malico.com
page: 3

Schlegel EMI
1600 Lexington Ave
Suite 236A
Rochester, NY 14606

t: 585-643-2000
e: schlegelemi.na@schlegelemi.com
w: www.schlegelemi.com
page: 23

SIEMENS Digital Industries Software
8005 SW Boeckman Road
Wilsonville, OR 97070

t: (800) 592-2210
e: www.plm.automation.siemens.com/global/en/contact-us.html
w: www.plm.automation.siemens.com/global/en/
page: C3

THERMAL LIVE
Online Event
October 19-20, 2021

t: (484) 688-0300
e: info@electronics-cooling.com
w: www.thermal.live
page: 34

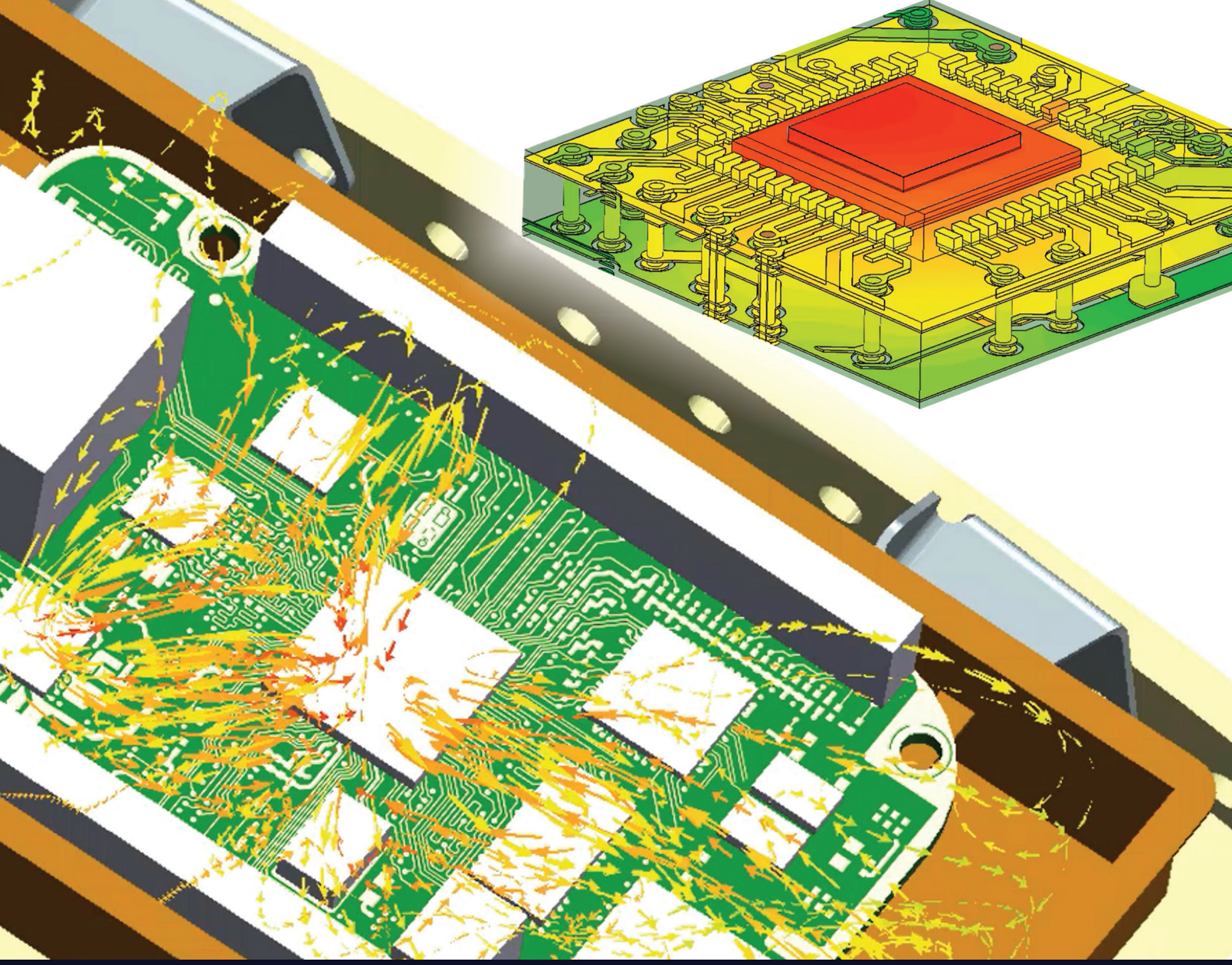

Enhance thermo-mechanical analysis workflows

Leverage efficient CFD to FEA worfklows for shorter, robust thermal and thermo-mechanical stress analysis. Discover how to create 3D transient temperature field results in CFD and map to an FEA mesh easily.

Simcenter portfolio includes leading electronics cooling software, CAD-embedded analysis, and multi-physics analysis tools to support a wider range of user skill and experience demographic from analyst to designer.

www.siemens.com/simcenter

SIEMENS


Break the same old pattern.
Problem First. Product Last.
Content | Data | Marketing Technology
LECTRIX®
Digital Marketing for the B2B Electronics Industry
1.484.688.0300 | info@lectrixgroup.com
www.lectrixgroup.com